INFORMATION TO USERS

This manuscript has been reproduced from the microfilm master. UMI films the text directly from the original or copy submitted. Thus, some thesis and dissertation copies are in typewriter face, while others may be from any type of computer printer.

The quality of this reproduction is dependent upon the quality of the copy submitted. Broken or indistinct print, colored or poor quality illustrations and photographs, print bleedthrough, substandard margins, and improper alignment can adversely affect reproduction.

In the unlikely event that the author did not send UMI a complete manuscript and there are missing pages, these will be noted. Also, if unauthorized copyright material had to be removed, a note will indicate the deletion.

Oversize materials (e.g., maps, drawings, charts) are reproduced by sectioning the original, beginning at the upper left-hand corner and continuing from left to right in equal sections with small overlaps. Each original is also photographed in one exposure and is included in reduced form at the back of the book.

Photographs included in the original manuscript have been reproduced xerographically in this copy. Higher quality 6" x 9" black and white photographic prints are available for any photographs or illustrations appearing in this copy for an additional charge. Contact UMI directly to order.

UMI

A Bell & Howell Information Company
300 North Zeeb Road, Ann Arbor MI 48106-1346 USA
313/761-4700 800/521-0600

AN EXTENDED NAMBU-JONA-LASINIO MODEL FOR HADRON INTERACTIONS

By

Wei Dong Sun

A dissertation submitted to Graduate Faculty in Physics in partial fulfillment of the requirements for the degree of Doctor of Philosophy, The City University of New York

1997

This manuscript has been read and accepted for the Graduate Faculty in Physics in satisfaction of the dissertation requirement for the degree of Doctor of Philosophy.

3-21-97
Date

Chair of Examining Committee

Date

Executive Officer

[Prof. L.S. Celenza]

[Prof. M. Kaku]

[Prof. H. Lancman]

[Prof. M.K. Liou]
Supervisory Committee

THE CITY UNIVERSITY OF NEW YORK

Abstract

AN EXTENDED NAMBU-JONA-LASINIO MODEL FOR HADRON INTERACTIONS

By

Wei Dong Sun

Adviser: Distinguished Professor Carl M. Shakin

We use the Nambu-Jona-Lasinio model to study the structure of mesons and the interaction of nucleons. A microscopic model of confinement is introduced to calculate various properties of hadrons. The confining interaction eliminates unphysical quark-antiquark cuts.

The model is used to calculated the nucleon-nucleon interaction for sigma, pion and vector-meson channels. It also calculates rho-omega mixing. An improvement is made for gauge invariance in the NJL model. Reasonable quantative results have been obtained.

Acknowledgements

To Professor Carl M. Shakin, my thesis advisor, I wish to express my deepest gratitude for his valuable guidance and constant encouragement throughout this work.

I would also like to express my sincere gratitude to Professor Louis S. Celenza for many useful discussions.

I wish to acknowledge with gratitude the Department of Physics of Brooklyn College and the Research Foundation of CUNY for the financial support during the course of this work.

CONTENTS

Chapter 1. Introduction

1.1 A Generalized NJL Model

The Nambu-Jona-Lasinio (NJL) model of 1961 was based on an analogy with the BCS theory. The model was later used as a dynamical theory for quarks.

The Lagrangian of the simple SU(2)-falvor version is

$$\begin{aligned}\mathcal{L}(x) &= \bar{q}(x)\left(i\gamma^{\mu}\partial_{\mu} - m_q^0\right)q(x) \\ &+ \frac{G_S}{2}\left[\left(\bar{q}(x)\,q(x)\right)^2 + \left(\bar{q}(x)\,i\gamma_5\,\vec{\tau}q(x)\right)^2\right] \\ &- \frac{G_V}{2}\left[\left(\bar{q}(x)\,\gamma_{\mu}\,\vec{\tau}q(x)\right)^2 + \left(\bar{q}(x)\gamma_{\mu}\gamma_5\,\vec{\tau}q(x)\right)^2\right] ,\end{aligned} \tag{1.1.1}$$

Here, m_q^0 is the current quark mass.

The low-lying mesons are found by solving the Bethe-Salpeter equation for the quark and antiquark systems. The T matrix in the scalar-isoscalar channel is

$$t_{qq}(t) = -\frac{G_S}{1 - G_S J_S(t)} \tag{1.1.2}$$

where, with $t = P^2$,

$$J_S(P^2) = (-1)n_c n_f i\int \frac{d^4k}{(2\pi)^3} iS_F(P/2 + k)iS_F(-P/2 + k) \tag{1.1.3}$$

is the basic quark-loop integral of the NJL model. [See Fig. 1.1.]

1.2 Confinement Interaction for Elimination of Unphysical Quark-antiquark Cuts.

In our generalized NJL model we introduced a model of confinement. That led to a modified form for $J_S(P^2)$. In Fig. 1.1(a) we show the summation of a ladder of confining interactions [Ce 95b]. We also define a vertex for the confining field that satisfies the equation shown in a schematic fashion in Fig. 1.2(b). Once the vertex function is calculated, we can replace $J_S(P^2)$ of Eq. (1.1.3) by $\hat{J}_S(P^2)$ shown in Fig. 1.2(b). Note that $\hat{J}_S(P^2)$ does not have an imaginary part which that would arise in a theory without confinement when both the quark and antiquark go on mass shell.

Chapter 2. Bosonization of the Extended NJL Model

2.1 Bosonization of Scalar-Isoscalar Mode

We will use a generalized version of the momentum-space bosonization scheme introduced in [Be 92]. There it is shown that one may write for the scalar-isoscalar channel,

$$-\frac{G_S}{1 - G_S J_S(q^2)} = \frac{g^2_{\sigma qq}(q^2)}{q^2 - m^2_\sigma(q^2)} \quad . \tag{2.1.1}$$

Explicit expressions are given for $J_S(q^2)$ and the momentum-dependent coupling constant and mass in [Be 92].

In our extended version of the NJL model, we replace $J_S(q^2)$ by $\hat{J}_S(q^2)$ and also include the amplitude $\hat{K}_S(q^2)$ shown in Fig 1.2 in the denominator of the T matrix in some cases. It is then useful to write $\hat{J}_S(q^2)$ as

$$\hat{J}_S(q^2) = s_1 - \frac{s_2}{q^2 - \bar{m}^2_\sigma} \tag{2.1.2}$$

where s_1, s_2 and $\bar{m}_\sigma$ are constants. (This form may be used for spacelike values of q^2, even if we do not find a pole in $\hat{J}_S(q^2)$ for $q^2 > 0$.) We now write

$$\hat{T}_S(q^2) = -\frac{1}{G_S^{-1} - \hat{J}_S(q^2)} \quad , \tag{2.1.3}$$

$$= -\frac{\left[\dfrac{q^2 - \tilde{m}_\sigma^2}{G_S^{-1} - s_1}\right]}{q^2 - \left[\tilde{m}_\sigma^2 - \dfrac{s_2}{G_S^{-1} - s_1}\right]} \quad . \tag{2.1.4}$$

Therefore, we may put

$$m_\sigma^2 = \tilde{m}_\sigma^2 - \frac{s_2}{G_S^{-1} - s_1} \quad , \tag{2.1.5}$$

and also define a momentum-dependent coupling constant (with $q^2 < \tilde{m}_\sigma^2$),

$$g_{\sigma qq}^2(q^2) = \frac{\tilde{m}_\sigma^2 - q^2}{G_S^{-1} - s_1} \quad , \tag{2.1.6}$$

which arises naturally in this formalism. Note that we will define $g_{\sigma qq}^2 = g_{\sigma qq}^2(0)$, with

$$g_{\sigma qq}^2(0) = \frac{\tilde{m}_\sigma^2}{G_S^{-1} - s_1} \quad . \tag{2.1.7}$$

With the various definitions given above, we have

$$\hat{T}_S(q^2) = \frac{g_{\sigma qq}^2(q^2)}{q^2 - m_\sigma^2} \quad . \tag{2.1.8}$$

We also see that

$$\frac{1}{G_S^{-1} - \hat{J}_S(0)} = \frac{g^2_{\sigma qq}(0)}{m^2_\sigma} \quad , \tag{2.1.9}$$

which is a useful relation for obtaining $g^2_{\sigma qq}$ from knowledge of G_S and $\hat{J}_S(0)$.

The situation in the case of the scalar-isoscalar channel is quite subtle, since the choice of parameters depends on the physical situation. For example, our studies have shown that, for spacelike values of q^2 near $q^2 = 0$, the value of m_σ in Eq. (2.1.8) is 540 MeV and $g_{\sigma qq}(0) = 2.58$, in one case [Ca 92]. However, there is no pole in the T matrix for $q^2 = m^2_\sigma$, with $m_\sigma = 540$ MeV. For example, as we will see, for timelike q^2 we find a pole at $q^2 = m^2_\sigma$, where $m_\sigma \simeq 900$ MeV, if $\kappa = 0.20$ GeV^2. One way to understand this point is to note that $J_S(q^2)$ and $\hat{J}_S(q^2)$ are quite similar for $q^2 < 0$, while these functions are quite different for timelike q^2. [See Fig. 2.1.] Note that the rapid rise of $J_S(q^2)$ for $q^2 > 0$ seen in Fig. 2.1 is due to the presence of a $q\bar{q}$ cut starting at $q^2 = 4m^2_q = 0.275$ GeV^2. Beyond that point $J_S(q^2)$ is complex. On the other hand, $\hat{J}_S(q^2)$ is everywhere real and a rapid rise in the value of that function could signal the presence of a bound state in the (linear) confining potential.

As a specific example, relevant to the spacelike region, consider the parameters $\tilde{m}^2_\sigma = 0.520$ GeV^2, $s_1 = 0.0479$ GeV^2 and $s_2 = 0.0178$ GeV^4. These values yield $m_\sigma = 0.540$ GeV, $g_{\sigma qq}(0) = 2.58$ and $\hat{J}_S(0) = 0.0821$ GeV^2. This parametrization describes the behavior of $\hat{J}_S(q^2)$ rather well for -0.3 GeV$^2 < q^2 < 0$: however, there is no pole at $\tilde{m}^2_\sigma = 0.520$ GeV^2 in the timelike region. (See Fig. 7 of [Sh 95 a].)

Note that, if we include $\hat{K}_S(q^2)$ in our considerations and use $\kappa = 0.22$ GeV^2,

we find $\hat{J}_S(0) + \hat{K}_S(0) = 0.0917$ GeV^2. Therefore, using $\hat{J}_S(0) + \hat{K}_S(0)$ instead of $\hat{J}_S(0)$ in Eq. (2.1.9),we find $g_{\sigma qq}(0) = 2.90$, if we again use $G_S = 7.91$ GeV^{-2} and $m_\sigma = 0.540$ GeV. This modification serves to enhance the magnitude of the T matrix at $q^2 = 0$ by about 27 percent relative to the result obtained when we neglect $\hat{K}_S(q^2)$. (We remark that an easy way to obtain Re $\hat{K}_S(q^2)$ is to calculate Im $\hat{K}_S(q^2)$ and then obtain Re $\hat{K}_S(q^2)$ by use of a dispersion relation [Ce 93 d].)

The rather complex situation that exists in the case of the sigma meson is greatly simplified when we consider the omega and rho mesons, since a single parametrization of the form of Eq. (2.1.2) may be used both in the spacelike and the timelike regions.

2.2. Bosonization for the Omega Meson

It is useful to divide the omega propagator and T matrix into transverse and longitudinal parts [Ce 95a]. For example, we may write

$$\frac{[g^{\mu\nu} - q^\mu q^\nu / m_\omega^2]}{q^2 - m_\omega^2} = \frac{[g^{\mu\nu} - q^\mu q^\nu / q^2]}{q^2 - m_\omega^2} - \frac{q^\mu q^\nu}{q^2 m_\omega^2} \quad . \tag{2.2.1}$$

One may also define the function $\hat{J}_{(\omega)}(q^2)$, related to a tensor $\hat{J}^{\mu\nu}_{(\omega)}(q^2)$. Here,

$$\hat{J}^{\mu\nu}_{(\omega)}(q^2) = -\left[g^{\mu\nu} - \frac{q^\mu q^\nu}{q^2}\right]\hat{J}_{(\omega)}(q^2) \quad , \tag{2.2.2}$$

where [Ce 95a]

$$-i\hat{J}^{\mu\nu}_{(\omega)}(q^2) = (-1)n_c n_f \mathrm{Tr}\int \frac{d^4k}{(2\pi)^4}\left[iS_F(q/2+k)\Gamma^\mu(q,k)\,iS_F(-q/2-k)\hat{\gamma}^\nu\right] \tag{2.2.3}$$

In this case $\Gamma^\mu(q, k)$ contains the vertex for the confining field and

$$\hat{\gamma}^\nu \equiv \gamma^\nu - \not{q} q^\nu / q^2 \quad . \tag{2.2.4}$$

Note that $q_\mu \hat{J}^{\mu\nu}_{(\omega)}(q^2) = \hat{J}^{\mu\nu}_{(\omega)}(q^2) q_\nu = 0$ in accord with Eq. (2.2.2), since $q_\mu \Gamma^\mu = q_\mu \hat{\gamma}^\mu = 0$ [Ce 95a].

In Fig. 2.2 we show $\hat{J}_{(\omega)}(t)$ for $\kappa = 0.16$ GeV^2, $\kappa = 0.22$ GeV^2, and $\kappa = 0.28$ GeV^2. A vertical line drawn at $t = m_\omega^2$ intersects each of these curves at a point. The ordinate of that point then yields a value for $1/G_\omega$, since the (transverse) T matrix may be written

$$\hat{T}^{\mu\nu}_{(\omega)} = -[g^{\mu\nu} - q^{\mu}q^{\nu}/q^2]\hat{T}_{(\omega)}(q^2) \quad , \tag{2.2.5}$$

with

$$\hat{T}_{(\omega)}(q^2) = \frac{1}{\frac{1}{G_\omega} - \hat{J}_{(\omega)}(q^2)} \quad . \tag{2.2.6}$$

A particularly useful representation for $\hat{J}_{(\omega)}(q^2)$ that has a simple physical interpretation is given by

$$\hat{J}_{(\omega)}(q^2) = v_1 - \frac{v_2}{q^2 - \tilde{m}^2_\omega} \quad . \tag{2.2.7}$$

In terms of these parameters, we have

$$m^2_\omega = \tilde{m}^2_\omega - \frac{v_2}{G^{-1}_\omega - v_1} \tag{2.2.8}$$

and

$$g^2_{\omega qq}(0) = \frac{\tilde{m}^2_\omega}{G^{-1}_\omega - v_1} \quad . \tag{2.2.9}$$

For example, if $\kappa = 0.22$ GeV^2, we find that with $G_\omega = 7.86$ GeV^{-2}, $v_1 = 0.0284$ GeV^2, $v_2 = 0.0850$ GeV^4 and $\tilde{m}^2_\omega = 1.476$ GeV^2, we obtain an accurate representation of $\hat{J}_{(\omega)}(q^2)$ for $q^2 > 0$. This result may be understood by interpreting $\tilde{m}_\omega$ as the mass of a bound state in the linear confining potential. (Note that $\tilde{m}_\omega$ is obtained

in the absence of the short-range attraction parametrized by G_ω.) The introduction of the short-range interaction then moves the bound state down to m_ω = 0.783 GeV. As noted above, this situation is much simpler than that in the scalar-isoscalar channel, since m_ω of Eq. (2.2.8) is equal to 0.783 GeV in both the timelike and spacelike domains of q^2.

2.3. Bosonization for the Rho Meson

Here, the new feature relative to the previous section is the importance of a tensor that describes the coupling of $q\bar{q}$ states to the two-pion continuum [Ce 95a],

$$\hat{K}^{\mu\nu}_{(\rho)}(q^2) = -\left[g^{\mu\nu} - \frac{q^\mu q^\nu}{q^2}\right]\hat{K}_{(\rho)}(q^2) \quad , \tag{2.3.1}$$

in addition to the tensor

$$\hat{J}^{\mu\nu}_{(\rho)}(q^2) = -\left[g^{\mu\nu} - \frac{q^\mu q^\nu}{q^2}\right]\hat{J}_{(\rho)}(q^2) \quad . \tag{2.3.2}$$

The (transverse) T matrix is of the form

$$\hat{T}^{\mu\nu}_{(\rho)}(q^2) = -\left[g^{\mu\nu} - \frac{q^\mu q^\nu}{q^2}\right]\hat{T}_{(\rho)}(q^2) \quad , \tag{2.3.3}$$

with

$$\hat{T}_{(\rho)}(q^2) = \frac{1}{G_\rho^{-1} - [\hat{J}_{(\rho)}(q^2) - \hat{K}_{(\rho)}(q^2)]} \quad . \tag{2.3.4}$$

Since m_ρ^2 is known, we find the appropriate value of G_ρ by solving the equation

$$\frac{1}{G_\rho} - [\hat{J}_{(\rho)}(m_\rho^2) + \mathrm{Re}\,\hat{K}_{(\rho)}(m_\rho^2)] = 0 \quad . \tag{2.3.5}$$

Again, we may indicate how this solution appears in a graphical form. For example, in Fig 2.3, with $t = q^2$, we show $\hat{J}_{(\rho)}(q^2) + \mathrm{Re}\,\hat{K}_{(\rho)}(q^2)$ for various κ. (Note that $\hat{J}_{(\rho)}(q^2) = \hat{J}_{(\omega)}(q^2)$.) Figure 2.4 shows $\mathrm{Re}\,\hat{K}_{(\rho)}(t)$ for various value of κ. Since we have fixed $\kappa = 0.22$ GeV^2 in our study of the omega meson, we use that value here and find that $G_\rho = 7.12$ GeV^{-2} yields a rho meson with $m_\rho = 0.770$ GeV.

In this case, we put

$$\hat{J}_{(\rho)}(q^2) + \mathrm{Re}\,\hat{K}_{(\rho)}(q^2) = r_1 - \frac{r_2}{q^2 - \tilde{m}_\rho^2} \quad , \tag{2.3.6}$$

so that

$$m_\rho^2 = \tilde{m}_\rho^2 - \frac{r_2}{G_\rho^{-1} - r_1} \quad , \tag{2.3.7}$$

and

$$g_{\rho qq}^2(q^2) = \frac{\tilde{m}_\rho^2 - q^2}{G_\rho^{-1} - r_1} \quad , \tag{2.3.8}$$

in analogy to what was done for the omega meson. Again, $g_{\rho qq}^2 = g_{\rho qq}^2(0)$, with

$$g_{\rho qq}^2(0) = \frac{\tilde{m}_\rho^2}{G_\rho^{-1} - r_1} \quad . \tag{2.3.9}$$

A good fit to $\hat{J}_{(\rho)}(q^2) + \mathrm{Re}\,\hat{K}_{(\rho)}(q^2)$ for $q^2 \geq 0$ is obtained if $r_1 = 0.0304$ GeV^2, $r_2 = 0.0968$ GeV^4 and $\tilde{m}_\rho^2 = 1.476$ GeV^2. (As noted above, $G_\rho = 7.12$ GeV^{-2}.)

Chapter 3. Nucleon-Nucleon Interaction for the Pion and Sigma Channels

3.1 Pion Exchange

In Fig. 3.1a we represent meson exchange in the OBE model on the left-hand side of the figure. There, the open circles are the form factors of the OBE model that are of the (monopole) form

$$F_i^{OBE}(t) = \left[\frac{\Lambda_i^2 - m_i^2}{\Lambda_i^2 - t} \right] \tag{3.1.1}$$

for a meson of mass m_i and OBE cut-off Λ_i. On the right-hand side of Fig. 3.1a we represent the interaction in terms of the quark-quark interaction, T. We do not consider all possible diagrams, but isolate those diagrams that are of leading order in $1/n_c$ counting [Sh 95b]. The interaction in that case may be expressed in terms of the functions, $\hat{J}(q^2)$ and $\hat{K}(q^2)$, for the various mesons. For example, in Fig. 3.1b we show those interactions that lead to the use of

$$t_{qq}^{(\sigma)}(t) = - \frac{G_S}{1 - G_S \hat{J}_S(t)} \tag{3.1.2}$$

in the case of sigma exchange. To keep in mind that we sum only the leading diagrams, we denoted the quark-quark T matrix as t_{qq} in Fig. 3.1c and in Eq. (3.1.2).

With reference to Fig. 3.1, we write a scattering amplitude for pion exchange in the OBE model as

$$f_{\pi}^{OBE}(t) = \frac{g_{\pi NN}^2}{4\pi}\left[\frac{\Lambda_{\pi}^2 - m_{\pi}^2}{\Lambda_{\pi}^2 - t}\right]^2 \frac{1}{t - m_{\pi}^2} \quad , \tag{3.1.3}$$

$$= f_{\pi}^{OBE}(0)\, h_{\pi}^{OBE}(t) \quad . \tag{3.1.4}$$

In Eq. (3.1.3) we have included the form factors of the OBE model that appear at each pion-nucleon vertex. It is also useful to define

$$\frac{G_{\pi NN}^2}{4\pi} = \frac{g_{\pi NN}^2}{4\pi}\left[\frac{\Lambda_{\pi}^2 - m_{\pi}^2}{\Lambda_{\pi}^2}\right]^2 \quad , \tag{3.1.5}$$

with similar definitions for the sigma, rho and omega mesons. The amplitude corresponding to $f_{\pi}^{OBE}(t)$ in the NJL model is (see Fig. 3.1c),

$$f_{\pi}^{NJL}(t) = \frac{t_{qq}^{(\pi)}(t)}{4\pi}\left|\tilde{F}_{\pi}(t)\right|^2 \quad , \tag{3.1.6}$$

$$= f_{\pi}^{NJL}(0)\, h_{\pi}^{NJL}(t) \quad . \tag{3.1.7}$$

Here, $t_{qq}^{(\pi)}$ is the quark-quark scattering amplitude of the NJL model and $\tilde{F}_{\pi}(t)$ is a nucleon form factor defined such that

$$\tilde{F}_\pi(t)\bar{u}(\vec{p}+\vec{q},s')i\gamma_5 u(\vec{p},s)<t'\,|\,\vec{\tau}|\,t> \;=\; <\vec{p}+\vec{q},s',t'\,|\,\bar{q}(0)i\gamma_5\vec{\tau}q(0)\,|\,\vec{p},s,t>. \tag{3.1.8}$$

It is useful to introduce a monopole form for the nucleon form factor,

$$\tilde{F}_\pi(t) = \tilde{F}_\pi(0)\left[\frac{\lambda_\pi^2}{\lambda_\pi^2 - t}\right] \quad . \tag{3.1.9}$$

In a previous work [Sh 95b] we saw that, if we took $\lambda_\pi = 0.8$ GeV, there was excellent agreement of the functions $h_\pi^{NJL}(t)$ and $h_\pi^{OBE}(t)$. [See Fig. 3.2.] Here, we also consider the magnitude of the amplitude in addition to the q^2 dependence, so that we have to provide a value for $\tilde{F}_\pi(0)$. In an earlier work, we found $\tilde{F}_\pi(0) = 4.78$, when we calculated the form factor $\tilde{F}_\pi(t)$ in a covariant soliton model of the nucleon [Ce 85]. Near $t \simeq 0$, we may put $t_{qq}^{(\pi)}(t) = g_{\pi qq}^2/(t - m_\pi^2)$, so that, in our model,

$$f_\pi^{NJL}(0) = -\frac{g_{\pi qq}^2}{4\pi}\frac{[\tilde{F}_\pi(0)]^2}{m_\pi^2} \quad , \tag{3.1.10}$$

$$= -676 \text{ GeV}^{-2} \quad , \tag{3.1.11}$$

where we have used $g_{\pi qq} = 2.68$ and $\tilde{F}_\pi(0) = 4.78$, as found in our earlier work [Ca 92,Ce 95]. Noting that $\Lambda_\pi = 1.3$ GeV and $g_{\pi NN}^2/4\pi = 14.4$ in typical OBE model calculations [Ma 89], we have

$$f_\pi^{OBE}(0) = -727 \text{ GeV}^{-2} \quad , \tag{3.1.12}$$

which is only 8 percent greater than $f_\pi^{NJL}(0)$ given in Eq. (3.1.11). Thus, we see that for pion exchange we fit both the value of $G_{\pi NN}\left(G_{\pi NN} = g_{\pi qq}\tilde{F}_\pi(0) = 12.8\right)$ and the q^2 dependence of the amplitude up to $-q^2 \simeq 2$ GeV^2. However, if we try to calculate $\tilde{F}_\pi(t)$, we obtain a form factor that is too soft. For example, the quark wave function of [Ce 85] yields a dipole form for the form factor,

$$\tilde{F}_\pi(t) = \tilde{F}_\pi(0)\left[\frac{1}{1 - \frac{t}{0.36}}\right]^2 , \qquad (3.1.13)$$

where $\tilde{F}_\pi(0) = 4.78$ and t is in GeV^2 units. For a monopole fit, the effective vertex parameter would be about $\lambda_\pi = 0.43$ GeV, which may be compared to the value used above, $\lambda_\pi = 0.80$ GeV.

3.2 Sigma Exchange

To study sigma exchange we need the nucleon form factor, $F_S(t)$, defined by the relation

$$F_S(t)\,u(\vec{p}+q,s')\,u(\vec{p},s)\,\delta_{tt'} = <\vec{p}+\vec{q},s',t'\,|\,\bar{q}(0)q(0)\,|\,\vec{p},s,t> \quad . \quad (3.2.1)$$

We may write

$$f_\sigma^{OBE}(t) = \frac{g_{\sigma NN}^2}{4\pi}\left[\frac{\Lambda_\sigma^2 - m_\sigma^2}{\Lambda_\sigma^2 - t}\right]^2 \frac{1}{t-m_\sigma^2} \quad , \quad (3.2.2)$$

$$= f_\sigma^{OBE}(0)\,h_\sigma^{OBE}(t) \quad , \quad (3.2.3)$$

and

$$f_\sigma^{NJL}(t) = \frac{t_{qq}^{(\sigma)}(t)}{4\pi}[F_S(t)]^2 \quad . \quad (3.2.4)$$

Now

$$f_\sigma^{OBE}(0) = -\frac{g_{\sigma NN}^2}{4\pi}\left[\frac{\Lambda_\sigma^2 - m_\sigma^2}{\Lambda_\sigma^2}\right]^2 \frac{1}{m_\sigma^2} \quad , \quad (3.2.5)$$

while

$$= -\frac{G_{\sigma NN}^2}{4\pi}\frac{1}{m_\sigma^2} \quad , \tag{3.2.6}$$

$$f_\sigma^{NJL}(0) = -\frac{g_{\sigma qq}^2}{4\pi}\frac{1}{m_\sigma^2}[F_S(0)]^2 \quad . \tag{3.2.7}$$

Thus, we would like to have

$$G_{\sigma NN} = g_{\sigma qq}F_S(0) \quad . \tag{3.2.8}$$

We note that, if we include $\hat{K}_S(0)$ in the formalism, $g_{\sigma qq}(0) = 3.05$ in our most recent analysis. In an earlier work, we calculated $F_S(0) = 1.94$ [Ce 85], so that, from Eq. (3.3.8), we find $G_{\sigma NN} \simeq 5.9$. This value is in fair agreement with the phenomenological value, if we consider the case where the effects of excitation of the delta are treated explicitly in the OBE model. For example, consider Table B.1 of [Ma 89]. For model I listed there, we find $g_{\sigma NN}^2/4\pi = 6.32$, $\Lambda_\sigma = 1.5$ GeV and $m_\sigma = 550$ MeV. Therefore, for that case

$$\frac{G_{\sigma NN}^2}{4\pi} = \frac{g_{\sigma NN}^2}{4\pi}\left[\frac{\Lambda_\sigma^2 - m_\sigma^2}{\Lambda_\sigma^2}\right]^2 \tag{3.2.9}$$

$$= 4.73 \tag{3.2.10}$$

so that $G_{\sigma NN} = 7.71$ which is somewhat larger than the value of $G_{\sigma NN} \simeq 5.9$ given above. Of course, the result is quite sensitive to the value chosen for $F_S(0)$. (It is

possible that vertex corrections enhance $F_S(0)$ to yield a value closer to 3. Such a value would place our analysis in better accord with the phenomenology of the OBE model.)

Chapter 4. Calculation of the Nucleon-Nucleon Interaction Due to Vector-Meson Exchange

4.1 Electromagnetic Form Factors of the Nucleon

In this section we review a number of well known relations, with the aim of providing a phenomenological representation of the isoscalar and isovector form factors of the nucleon. We recall that proton and neutron form factors may be defined, with $e > 0$,

$$\left\langle \vec{p}', s', \tau' = 1/2 \left| J^{\mu}_{em}(0) \right| \vec{p}, s, \tau = 1/2 \right\rangle = e\bar{u}(\vec{p}', s') \left[\gamma^{\mu} F_1^p(q^2) + \frac{i\sigma^{\mu\nu}}{2m_N} q_\nu F_2^p(q^2) \right] u(\vec{p}, s) \quad , \tag{4.1.1}$$

$$\left\langle \vec{p}', s', \tau' = -1/2 \left| J^{\mu}_{em}(0) \right| \vec{p}, s, \tau = -1/2 \right\rangle = e\bar{u}(\vec{p}', s') \left[\gamma^{\mu} F_1^n(q^2) + \frac{i\sigma^{\mu\nu}}{2m_N} q_\nu F_2^n(q^2) \right] u(\vec{p}, s) \quad . \tag{4.1.2}$$

Here $\vec{p}' = \vec{p} + \vec{q}$.

One further defines electric and magnetic form factors

$$G_E^p(q^2) = F_1^p(q^2) + \frac{q^2}{4m_N^2} F_2^p(q^2) \quad , \tag{4.1.3}$$

$$G_M^p(q^2) = F_1^p(q^2) + F_2^p(q^2) \quad , \tag{4.1.4}$$

and

$$G_E^n(q^2) = F_1^n(q^2) + \frac{q^2}{4m_N^2} F_2^n(q^2) \quad , \tag{4.1.5}$$

$$G_M^n(q^2) = F_1^n(q^2) + F_2^n(q^2) \quad . \tag{4.1.6}$$

We also put

$$F_1^p(q^2) = F_1^S(q^2) + F_1^V(q^2) \quad , \tag{4.1.7}$$

$$F_2^p(q^2) = F_2^S(q^2) + F_2^V(q^2) \quad , \tag{4.1.8}$$

$$F_1^n(q^2) = F_1^S(q^2) - F_2^V(q^2) \quad , \tag{4.1.9}$$

and

$$F_2^n(q^2) = F_2^S(q^2) - F_2^V(q^2) \quad . \tag{4.1.10}$$

We then solve for the isoscalar and isovector form factors

$$F_1^S(q^2) = \frac{G_E^p(q^2) + G_E^n(q^2) - (q^2/4m_N^2)\,(G_M^p(q^2) + G_M^n(q^2))}{2(1 - q^2/4m_N^2)} \quad , \tag{4.1.11}$$

$$F_2^S(q^2) = \frac{\left[G_M^p(q^2) + G_M^n(q^2)\right] - \left[G_E^p(q^2) + G_E^n(q^2)\right]}{2(1 - q^2/4m_N^2)} \quad , \tag{4.1.12}$$

and

$$F_1^V(q^2) = \frac{\left[G_E^p(q^2) - G_E^n(q^2)\right] - (q^2/4m_N^2)\left[G_M^p(q^2) - G_M^n(q^2)\right]}{2(1 - q^2/4m_N^2)} \quad . \qquad (4.1.13)$$

$$F_2^V(q^2) = \frac{\left[G_M^p(q^2) - G_M^n(q^2)\right] - \left[G_E^p(q^2) - G_E^n(q^2)\right]}{2(1 - q^2/4m_N^2)} \quad . \qquad (4.1.14)$$

We remark that $F_1^S(0) = 0.5$, $F_2^S(0) = -0.06$, $F_1^V(0) = 0.5$ and $F_2^V(0) = 1.85$. For the range of momentum of interest to us, we may use the dipole forms (with q^2 in GeV^2 units),

$$G_E^p(q^2) = \frac{1}{\left[1 - \frac{q^2}{0.71}\right]^2} \quad , \qquad (4.1.15)$$

$$G_M^p(q^2) = \mu_p G_E^p(q^2) \quad , \qquad (4.1.16)$$

$$G_M^n(q^2) = \mu_n G_E^p(q^2) \quad . \qquad (4.1.17)$$

Here, $\mu_p = 2.79$, $\mu_n = -1.91$ and $G_E^n(q^2) \simeq 0$. Use of Eqs. (4.1.15)-(4.1.17) in Eqs. (4.1.11)-(4.1.14) provides a phenomenological representation of the isoscalar and isovector form factors. We will describe a procedure for obtaining theoretical values for $F_1^S(q^2)$ and $F_2^V(q^2)$ in the next section.

4.2. The Vector-Meson-Dominance Model for the Nucleon Electromagnetic Form Factors

It is well known that hadron electromagnetic form factors may be calculated in some form of the vector-meson-dominance (VMD) model. (Indeed, the VMD model provides a remarkably accurate representation of the pion form factor for both timelike and spacelike values of q^2[Sh 97a,Fr95].) Here, we will develop a version of the VMD model for the nucleon electromagnetic form factors that will provide some information needed in the calculation of rho and omega exchange in our study of the nucleon-nucleon interaction.

We will not use the bag model in our analysis; however, we do have in mind a picture of the nucleon as a valence-quark "core" strongly coupled to surrounding meson fields. From this point of view, we may consider the processes shown in Fig. 4.1. There the wavy line denotes a photon, the single lines are quarks and the cross-hatched area represents the "valence-quark core". In Fig. 4.1a the photon is absorbed by a quark in the core. The process shown in Fig. 4.1a gives rise to an isoscalar amplitude

$$A^{\mu}(p,p') = \frac{e}{2}\bar{u}(\vec{p}',s')\left[\gamma^{\mu}f_1^S(q^2) + \frac{i\sigma^{\mu\nu}}{2m_N}q_{\nu}f_2^S(q^2)\right]u(\vec{p},s) \qquad (4.2.1)$$

where $f_1^S(q^2)$ and $f_2^S(q^2)$ are form factors of the core. In Figs. 4.1a and 4.1b, we see the photon being absorbed,with subsequent rescattering of the quark-antiquark pair. (Note that we do not show the confinement vertex in these figures to avoid excessive complexity in the figure.) Inclusion of the full series of $q\bar{q}$ "bubbles", as shown in Figs.

4.1a, 4.1b, 4.1c, etc., yields the amplitude in the omega channel $J = 1^-, I = 0$)

$$B^{\mu}_{(\omega)}(p', p) = \frac{e}{2} \frac{1}{1 - G_{\omega}\left[\hat{J}_{(\omega)}(q^2) + \hat{K}_{(\omega)}(q^2)\right]} \bar{u}(\vec{p}', s') \left[\gamma^{\mu} f_1^S + \frac{i\sigma^{\mu\nu}}{2m_N} q_{\nu} f_2^S\right] u(\vec{p}, s) \tag{4.2.2}$$

From this form we may identify the VMD result by using our bosonization relations. We find

$$B^{\mu}_{(\omega)}(p', p) = \frac{e}{2} \frac{1}{G_{\omega}} \frac{g^2_{\omega qq}(q^2)}{m^2_{\omega} - q^2} \bar{u}(p', s') \left[\gamma^{\mu} f_1^S + \frac{i\sigma^{\mu\nu} q_{\nu}}{2m_N} f_2^S\right] u(\vec{p}, s) \tag{4.2.3}$$

This may be put in a somewhat more familiar form by defining a meson decay constant $g^{\omega}(q^2)$ [Sh 97a,Fr 95]:

$$\frac{m^2_{\omega}}{g^{\omega}(q^2)} = \frac{g_{\omega qq}(q^2)}{6G_{\omega}} \tag{4.2.4}$$

Thus,

$$B^{\mu}_{(\omega)}(p', p) = e\left[\frac{m^2_{\omega}}{g^{\omega}(q^2)}\right] \frac{1}{m^2_{\omega} - q^2} g_{\omega qq}(q^2)\, \bar{u}(\vec{p}', s') \left[\gamma^{\mu} f_1^S + \frac{i\sigma^{\mu\nu}}{2m_N} q_{\nu} f_2^S\right] u(\vec{p}, s) \tag{4.2.5}$$

Thus, we may identify isoscalar form factors of the nucleon

$$F_1^S(q^2) = \frac{1}{6G_{\omega}} \frac{g^2_{\omega qq}(q^2)}{m^2_{\omega} - q^2} f_1^S(q^2) \quad , \tag{4.2.6}$$

$$F_2^S(q^2) = \frac{1}{6G_\omega} \frac{g^2_{\omega qq}(q^2)}{m_\omega^2 - q^2} f_2^S(q^2) \quad , \tag{4.2.7}$$

For definiteness, we can define $f_1^S(0) = 3$ and require that $f_2^S(0) = -0.12$. (Since $f_2^S(0)$ is quite small, we will neglect it at this point.) We may use $G_\omega = 7.86\ \text{GeV}^{-2}$, $m_\omega = 0.783\ \text{GeV}$, and $g_{\omega qq}(0) = 3.86$, and find $F_1^S(0) = 0.5$.

For the isovector form factors, entirely similar considerations allow us to write,

$$F_1^V(q^2) = \frac{1}{2G_\rho} \frac{g^2_{\rho qq}(q^2)}{m_\rho^2 - q^2} f_1^V(q^2) \quad , \tag{4.2.8}$$

$$F_2^V(q^2) = \frac{1}{2G_\rho} \frac{g^2_{\rho qq}(q^2)}{m_\rho^2 - q^2} f_2^V(q^2) \quad , \tag{4.2.9}$$

Here, we require $f_1^V(0) = 1$ and $f_2^V(0) = 3.70$, so that $F_1^V(0) = 0.5$ and $F_2^V(0) = 1.85$.

The choice of $f_2^S(0) = -0.12$ and $f_2^V(0) = 3.70$ may seem somewhat arbitrary. However, we have seen in past work that, if one uses a relativistic version of the SU(6) quark-model wave functions of the nucleon, it is quite easy to fit these values in what may be considered to be a pure "core" model [Ce 85]. That is, in [Ce 85], we did not use the VMD model, nor did we consider the contribution of the "meson cloud". The success of that analysis was based on the fact that, if one calculates the matrix element of the isoscalar current, $j_S^\mu(x) = \bar{q}(x)\gamma^\mu q(x)$, between nucleon states, the resulting value of $f_2^S(0)$ is quite small. On the other hand, if one calculates the matrix element of the isovector current, $j_V^\mu(x) = \bar{q}(x)\gamma^\mu \tau_3 q(x)$, a large value of $f_2^V(0)$ is obtained. Indeed, the moments of the neutron and proton were very well fitted by the simple "core" model of

[Ce 85]. However, in the present work we have used a VMD model and a nucleon "core" to facilitate our study of the nucleon-nucleon force due to vector-meson exchange.

The purpose of the foregoing analysis was to find some information concerning the core form factors. To that end, we put

$$f_1^V(q^2) = \frac{(\lambda_1^V)^2}{(\lambda_1^V)^2 - q^2} \quad , \tag{4.2.10}$$

$$f_2^V(q^2) = 3.70 \frac{(\lambda_2^V)^2}{(\lambda_2^V)^2 - q^2} \quad , \tag{4.2.11}$$

$$f_1^S(q^2) = 3 \frac{(\lambda_1^S)^2}{(\lambda_1^S)^2 - q^2} \quad , \tag{4.2.12}$$

$$f_2^S(q^2) = -0.12 \frac{(\lambda_2^S)^2}{(\lambda_2^S)^2 - q^2} \quad . \tag{4.2.13}$$

At this point, we may find values of the various λ's by using the phenomenological values of F_1^S, F_2^S, F_1^V and F_2^V given in Section III. We will concentrate on $F_1^S(q^2)$ and $F_2^V(q^2)$, since these form factors appear in the most important components of the nucleon-nucleon interaction that arise from vector-meson exchange. In Fig. 4.2 we show a fit to $F_1^S(q^2)$ obtained with $\lambda_1^S = 0.745$ GeV and in Fig. 4.3 we show a fit to $F_2^V(q^2)$ obtained with $\lambda_2^V = 0.70$ GeV. (If we convert these

values of λ to a "core radius" by using the formula $R = \sqrt{6} / \lambda$, we find $R_\rho \simeq 0.69$ fm and $R_\omega \simeq 0.65$ fm. (These values represent about 80 percent of the value of the electromagnetic radius of the nucleon.)

4.3. Vector-Meson Exchange in the OBE Model

The one-boson-exchange model provides a particularly simple representation of the nucleon-nucleon interaction [Ma 89]. One characteristic of the model is the inclusion of a vertex cutoff at each meson-nucleon vertex. For the monopole form of the vertex cutoff, we have, for meson i,

$$\mathcal{F}_i^{OBE}(q^2) = \frac{\Lambda_i^2 - m_i^2}{\Lambda_i^2 - q^2} \tag{4.3.1}$$

at each vertex. For example, for omega exchange, one has an amplitude

$$f_{(\omega)}^{OBE}(q^2) = \frac{g_{\omega NN}^2}{4\pi}\left[\frac{\Lambda_\omega^2 - m_\omega^2}{\Lambda_\omega^2 - q^2}\right]^2 \frac{1}{m_\omega^2 - q^2} \quad . \tag{4.3.2}$$

Here, $g_{\omega NN}$ is the omega-nucleon coupling constant as defined in [Ma 89]. We have included a factor of $(1/4\pi)$ in Eq. (4.3.2), since the value of the coupling constant is usually given by specifying the value of $g^2/4\pi$. For example, we have $g_{\omega NN}^2/4\pi = 20.0$ and $\Lambda_\omega = 1.5$ GeV as typical values in the OBE model [Ma 89]. From these values, we have $f_{(\omega)}^{OBE} = 17.26\ \text{GeV}^{-2}$, if we use the definition of $f_{(\omega)}^{OBE}(q^2)$ given in Eq. (4.3.2).

To calculate the corresponding amplitude in the extended NJL model, we consider the diagrams of Fig. 4.4. Note that to obtain an expression similar to that of the OBE model, we may consider the interaction of the valence quark "cores" that were introduced in the last section. For example, we may write, for omega exchange,

$$\Gamma^{\mu}_{NJL} = \bar{u}(\vec{p}_2 - \vec{q}, s_2')\left[\gamma^{\mu} f_1^S(q^2) - \frac{i\sigma^{\mu\nu}}{2m_N} q_\nu f_2^S(q^2)\right] u(\vec{p}_2, s_2) \frac{G_\omega}{1 - G_\omega \hat{J}_{(\omega)}(q^2)}$$
$$\times \bar{u}(\vec{p}_1 + \vec{q}, s_1')\left[\gamma^{\mu} f_1^S(q^2) + \frac{i\sigma^{\mu\nu}}{2m} q_\nu f_2^S(q^2)\right] u(\vec{p}_1, s_1) \quad . \tag{4.3.3}$$

We now use our basic bosonization relations to extract the amplitude proportion to $[f_1^S(q^2)]^2$. We again insert a factor of $(1/4\pi)$ and write

$$f^{NJL}_{(\omega)}(q^2) = \frac{1}{4\pi} \frac{g^2_{\omega qq}(q^2)}{m_\omega^2 - q^2} \left[f_1^S(q^2)\right]^2 \quad , \tag{4.3.4}$$

$$= \frac{1}{4\pi} t^{(\omega)}_{qq}(q^2) \left[\frac{(\lambda_1^S)^2}{(\lambda_1^S)^2 - q^2}\right]^2 \left[f_1^S(0)\right]^2 \quad , \tag{4.3.5}$$

where we have put $t^{(\omega)}_{qq}(q^2) = g^2_{\omega qq}(q^2)/(m_\omega^2 - q^2)$ and made use of Eq. (4.2.12). With $\lambda_1^S = 0.745$ GeV, $g_{\omega qq}(0) = 3.86$ (see Table 4.1) and $f_1^S(0) = 3.0$, we obtain $f^{NJL}_{(\omega)}(0) = 17.4$ GeV^{-2}, which is close to the value $f^{OBE}_{(\omega)}(0) = 17.3$ GeV^{-2} calculated above. The functions $f^{NJL}_{(\omega)}(q^2)$ and $f^{OBE}_{(\omega)}(q^2)$ are compared in Fig. 4.5. We see that $f^{NJL}_{(\omega)}(q^2)$ falls off more quickly than $f^{OBE}_{(\omega)}(q^2)$ as $-q^2$ is increased.

We now turn to a consideration of rho exchange. Here we will concentrate on the tensor component of the force. In the OBE model, we consider the amplitude

$$f_{(\rho)}^{OBE}(q^2) = \frac{f_{\rho NN}^2}{4\pi}\left[\frac{\Lambda_\rho^2 - m_\rho^2}{\Lambda_\rho^2 - q^2}\right]^2 \frac{1}{m_\rho^2 - q^2} \quad , \tag{4.3.6}$$

where $f_{\rho NN}$ is related to $g_{\rho NN}$ by $f_{\rho NN}/g_{\rho NN} = 6.1$ [Ma 89]. The coupling constants are used to parametrize the form of the meson-nucleon vertex in the OBE model. For example, the vertex for rho-nucleon coupling is [Ma 89]

$$\Gamma_{OBE}^{\mu} = \bar{u}(\vec{p}+\vec{q}, s')\left[g_{\rho NN}\gamma^{\mu} + f_{\rho NN}\frac{i\sigma^{\mu\nu}q^{\nu}}{2m_N}\right]u(\vec{p}, s) < \tau' \mid \tau_3 \mid \tau > \left[\frac{\Lambda_\rho^2 - m_\rho^2}{\Lambda_\rho^2 - q^2}\right] \quad . \tag{4.3.7}$$

Here, we see that, in the case of the OBE model, the same value of Λ_ρ is used in the central and the tensor term. We have $g_{\rho NN}^2/4\pi = 0.99$ and $\Lambda_\rho = 1.3$ GeV as typical values in the OBE model [Ma 89]. Thus, $f_{\rho NN}^2/4\pi = 36.8$ and, from Eq. (4.3.6), we find $f_{(\rho)}^{OBE}(0) = 26.2$ GeV^{-2}.

The NJL amplitude is obtained by considering an expression analogous to Eq. (4.3.3),

$$\Gamma^{\mu}_{NJL} = \bar{u}(\vec{p}_2 - \vec{q}, s_2') \left[\gamma^{\mu} f_1^{V}(q^2) - \frac{i\sigma^{\mu\nu} q^{\nu}}{2m_N} f_2^{V}(q^2) \right] u(\vec{p}_2, s_2) \frac{G_{\rho}}{1 - G_{\rho}\left[\hat{J}_{(\rho)}(q^2) + \hat{K}_{(\rho)}(q^2) \right]}$$

$$\times \bar{u}(\vec{p}_1 + \vec{q}, s_1') \left[\gamma^{\mu} f_1^{V}(q^2) + \frac{i\sigma^{\mu\beta} q_{\beta}}{2m_N} f_2^{V}(q^2) \right] u(\vec{p}_1, s_1) \quad . \tag{4.3.8}$$

In Eq. (4.3.8) we have not written the isospin factors, for simplicity. Thus,

$$f_{(\rho)}^{NJL}(q^2) = \frac{1}{4\pi} \frac{G_{\rho}}{1 - G_{\rho}\left[\hat{J}_{(\rho)}(q^2) + \hat{K}_{(\rho)}(q^2) \right]} \left[f_2^{V}(q^2) \right]^2 \quad , \tag{4.3.9}$$

$$= \frac{1}{4\pi} \frac{g_{\rho qq}^2(q^2)}{m_{\rho}^2 - q^2} \left[f_2^{V}(q^2) \right]^2 \quad , \tag{4.3.10}$$

$$= \frac{1}{4\pi} t_{qq}^{(\rho)}(q^2) \left[\frac{(\lambda_2^{V})^2}{(\lambda_2^{V})^2 - q^2} \right]^2 \left[f_2^{V}(0) \right]^2 \quad . \tag{4.3.11}$$

Noting that $g_{\rho qq}(0) = 3.66$, $f_2^{V}(0) = 3.70$, and $m_{\rho} = 0.77$ GeV, we find $f_{(\rho)}^{NJL}(0) = 24.6$ GeV^{-2}, which is 94 percent of the corresponding OBE result. [See Fig. 4.6.]

Chapter 5. Many-Body Theory of Rho-Omega Mixing

5.1. Introduction

In this work we will use a generalized Nambu−Jona-Lasinio (NJL) model [Na 61,Ce 95a,d] to calculate the polarization tensor that describes rho-omega mixing. That quantity has been of some interest in recent years, since the value of the tensor at $q^2 = m_\omega^2$ was used to estimate one form of charge symmetry breaking (CSB) in the nucleon-nucleon force. However, it was pointed out by several authors that for the calculation of the nucleon-nucleon force one needs the tensor for spacelike q^2, that is $q^2 \leq 0$ [Go 92]. It was found that the relevant matrix element is small at $q^2 = 0$ and, therefore, ρ-ω mixing was seen to be unimportant in the calculation of CSB. Therefore, the motivation for studying ρ-ω mixing is diminished. However, there are a number of interesting theoretical issues associated with the calculation of the mixing that have not been fully resolved. One problem that arises is the ambiguity associated with the definition of the rho and omega interpolating fields. For example, Cohen and Miller [Co 95] point out that it is possible to shift CSB effects from the mixed ρ-ω propagator to the meson-nucleon vertex functions. This leads, of course, to significant ambiguities. To a large degree these ambiguities can be avoided by working at the quark level and calculating the current correlator of isoscalar and isovector vector currents. That program has been carried out in [Ha 94,Iq 95] using QCD sum-rule techniques.

We may also use quark degrees of freedom to perform a calculation of the current correlator of isovector and isoscalar currents using the NJL model. It should be clear, however, that if we use the NJL model, we need a model for confinement. We have

extended the NJL model to include a description of confinement [Ce 93a,d] and will use that model in this work. The Lagrangian of our model is

$$\begin{aligned}\mathcal{L}(x) &= \bar{q}(i\partial - m_q^0)q + \frac{G_S}{2}[(\bar{q}q)^2 + (\bar{q}i\gamma_5\vec{\tau}q)^2] \\ &- \frac{G_\rho}{2}[(\bar{q}\gamma^\mu\vec{\tau}q)^2 + (\bar{q}\gamma_5\gamma_\mu\vec{\tau}q)^2] \\ &- \frac{G_\omega}{2}(\bar{q}\gamma^\mu q)^2 + \mathcal{L}_{conf}(x) \quad ,\end{aligned} \tag{5.1.1}$$

which we present here in order to define the coupling constants, G_ρ and G_ω, which appear in our discussion. (Work somewhat related to ours has been reported in [Mi 94], where confinement is implemented in a Euclidean-momentum-space analysis of a global color model.)

The organization of our work is as follows. In Section 5.2 we introduce various current correlators and the associated vector currents. We also relate the omega and rho fields to these currents. In Section 5.3 we discuss the momentum-space bosonization of the extended NJL model and calculate the fundamental matrix element that parametrizes the on-shell ($q^2 = m_\omega^2$) ρ-ω mixing. In Section 5.4 we relate the ρ and ω decay constants to the rho-quark and omega-quark coupling constants that we have calculated in an earlier work. In Section 5.5 we describe a subtracted current correlation function that vanishes at $q^2 = 0$. Finally, Section 5.6 contains some further discussion and conclusions. We also give the value of the current quark mass difference $m_d^0 - m_u^0$ that leads to a fit to the experimental data.

5.2. Calculation of Current-Current Correlation Functions

We find it useful to start our discussion with the definition made by Maltman [Ma 95]. He defines a mixed propagator for rho and omega fields in vacuum,

$$\Pi_{\mu\nu}^{(\rho\omega)}(q^2) = i\int d^4x e^{iq\cdot x} < T(\rho_\mu(x)\omega_\nu(0)) > \quad , \tag{5.2.1}$$

$$= \left[g_{\mu\nu} - \frac{q_\mu q_\nu}{q^2} \right] \frac{\theta(q^2)}{(q^2 - m_\rho^2 + i\epsilon)(q^2 - m_\omega^2 + i\epsilon)} \quad , \tag{5.2.2}$$

where $\theta(q^2)$ is the function to be determined. At $q^2 = m_\omega^2$, $\theta(q^2)$ is proportional to the matrix element $< \rho \mid H_{SB} \mid \omega >$ [Mc 75]. In this work we will exhibit the relation between $\theta(m_\omega^2)$ and

$< \rho \mid H_{SB} \mid \omega >$ for the choice of omega and rho fields that we will use here. (In some studies the definition of the fields is such that $\theta(m_\omega^2)$ may be taken equal to $< \rho \mid H_{SB} \mid \omega >$ [Ha 94,Iq 95].)

It has been pointed out that the widths of the rho and omega mesons must be included, if we wish to obtain the correct q^2 dependence of $\theta(q^2)$ [Iq 95]. Therefore, we use the definition of $\theta_3(q^2)$ of [Iq 95]. That is, Eq. (5.2.2) is modified to read

$$\Pi_{\mu\nu}^{(\rho\omega)}(q) = \hat{g}_{\mu\nu}(q) \frac{\theta_3(q^2)}{\left[q^2 - \left[m_\rho - \frac{i\Gamma_\rho}{2} \right]^2 \right] \left[q^2 - \left[m_\omega - \frac{i\Gamma_\omega}{2} \right]^2 \right]} \quad , \tag{5.2.3}$$

with

$$\hat{g}_{\mu\nu}(q) = g_{\mu\nu} - q_\mu q_\nu / q^2 \quad . \tag{5.2.4}$$

The functions Γ_ρ and Γ_ω are q^2-dependent with the values $\Gamma_\omega(m_\omega^2) = 8.4$ MeV and

$\Gamma_\rho(m_\rho^2) = 151.5$ MeV. (The omega width is small, since two-pion decay of the omega violates G parity.)

As mentioned in the introduction to this section, some of the recent literature deals with the fact that the interpolating fields, $\rho_\mu(x)$ and $\omega_\mu(x)$, are not fixed, but may be transformed in many ways without changing the values of the S matrices of the theory [Co 95,Ma 95]. Because of that ambiguity, it is found that CSB effects may be transferred from propagators to vertex functions and visa versa. Therefore, it is important to define the omega and rho fields in a definite scheme and relate that definition to the underlying quark degrees of freedom. The most natural choice is to define these fields via a momentum-space bosonization procedure [Be 92]. In that case, the fields are proportional to the isoscalar and isovector electromagnetic currents [Ma 95],

$$j_\mu^S(x) = \frac{1}{6}\bar{q}(x)\gamma_\mu q(x) \quad , \tag{5.2.5}$$

and

$$j_\mu^V(x) = \frac{1}{2}\bar{q}(x)\gamma_\mu \tau_3 q(x) \quad . \tag{5.2.6}$$

Therefore, instead of working with Eq. (5.2.1), we define

$$\hat{\Pi}_{\mu\nu}^{(\rho\omega)}(q) = i\int d^4x e^{iq\cdot x}\left\langle T\left(j_\mu^V(x) j_\nu^S(0)\right)\right\rangle \quad . \tag{5.2.7}$$

We also introduce currents

$$J_\mu^S(x) = \bar{q}(x)\gamma_\mu q(x) \quad , \tag{5.2.8}$$

and

$$J_\mu^V(x) = \bar{q}(x)\gamma_\mu\tau_3 q(x) \quad . \tag{5.2.9}$$

We then define

$$\tilde{\Pi}_{\mu\nu}^{(\rho\omega)}(q) = i\int d^4x e^{iq\cdot x}\left\langle T\left(J_\mu^V(x)J_\nu^S(0)\right)\right\rangle \quad , \tag{5.2.10}$$

where

$$\tilde{\Pi}_{\mu\nu}^{(\rho\omega)}(q) = 12\hat{\Pi}_{\mu\nu}^{(\rho\omega)}(q) \quad . \tag{5.2.11}$$

The reason for introducing $\tilde{\Pi}_{\mu\nu}^{(\rho\omega)}(q)$ is that it lends itself to a more transparent diagrammatic analysis. For completeness, we also define

$$\hat{\Pi}_{\mu\nu}^{(\rho)}(q) = i\int d^4x e^{iq\cdot x}\left\langle T\left(j_\mu^V(x)j_\nu^V(0)\right)\right\rangle \quad , \tag{5.2.12}$$

$$= -\hat{g}_{\mu\nu}(q)\,\hat{\Pi}^{(\rho)}(q^2) \quad , \tag{5.2.13}$$

and

$$\hat{\Pi}_{\mu\nu}^{(\omega)}(q) = i\int d^4x e^{iq\cdot x}\left\langle T\left(j_\mu^S(x)j_\nu^S(0)\right)\right\rangle \quad , \tag{5.2.14}$$

$$= -\hat{g}_{\mu\nu}(q)\,\hat{\Pi}^{(\omega)}(q^2) \quad . \tag{5.2.15}$$

Let us write

$$\tilde{\Pi}_{\mu\nu}^{(\rho\omega)}(q) = \hat{g}_{\mu\nu}(q)\,\frac{\tilde{\theta}_3(q^2)}{\left[q^2-\left(m_\rho-\frac{i\Gamma_\rho}{2}\right)^2\right]\left[q^2-\left(m_\omega-\frac{i\Gamma_\omega}{2}\right)^2\right]} \quad , \tag{5.2.16}$$

so that we now need to specify the relation between $\theta_3(q^2)$ of Eq. (5.2.5) and $\tilde{\theta}_3(q^2)$ of Eq. (5.2.16). A simple way to do that is to relate the ρ and ω fields to the isoscalar and isovector currents as in [8],

$$\rho^\mu(x) = \frac{g^\rho}{m_\rho^2} j_V^\mu(x) \tag{5.2.17}$$

and

$$\omega^\mu(x) = \frac{g^\omega}{m_\omega^2} j_S^\mu(x) \quad . \tag{5.2.18}$$

Here, g^ρ and g^ω are rho and omega decay constants, defined such that the matrix elements of the current between the vacuum and the vector meson states are

$$\left\langle 0 \left| j_V^\mu \right| \rho(q, \epsilon_\lambda) \right\rangle = \frac{m_\rho^2}{g^\rho} \epsilon_\lambda^\mu(q) \quad , \tag{5.2.19}$$

and

$$\left\langle 0 \left| j_S^\mu \right| \omega(q, \epsilon_\lambda) \right\rangle = \frac{m_\omega^2}{g^\omega} \epsilon_\lambda^\mu(q) \quad . \tag{5.2.20}$$

Here, $\epsilon_\lambda^\mu(q)$ is a polarization four vector. (At this point, we note the difference between g^ρ and g^ω and the meson-quark coupling constants, such as $g_{\omega qq}$ and $g_{\rho qq}$, that describe omega-quark and rho-quark coupling, respectively. See Section 5.3.)

It follows that

$$\theta_3(q^2) = \frac{g^\rho g^\omega}{12 m_\rho^2 m_\omega^2} \tilde{\theta}_3(q^2) \quad , \tag{5.2.21}$$

if we assume that the isoscalar and isovector currents couple predominantly to the low-

lying omega and rho fields. Note that, when we use Eqs. (5.2.19) and (5.2.20), the rho and omega mesons are on-mass-shell. Therefore, while $\bar{\theta}_3(q^2)$ is well-defined for all q^2, the off-mass-shell behavior of $\theta_3(q^2)$ is somewhat arbitrary. If so desired, it is possible to carry out the entire analysis for $\bar{\theta}_3(q^2)$ only.

5.3 Bosonization for Omega and Rho Fields

Consider the calculation of $\tilde{\Pi}^{(\rho\omega)}_{\mu\nu}(q)$. That may be done in terms of fundamental quark-loop integrals of the NJL model. We define tensors [Ce 95a]

$$\hat{J}^{\mu\nu}_{(\rho)}(q) = -\hat{g}^{\mu\nu}(q)\hat{J}_{(\rho)}(q^2) \quad , \tag{5.3.1}$$

and

$$\hat{J}^{\mu\nu}_{(\omega)}(q) = -\hat{g}^{\mu\nu}(q)\hat{J}_{(\omega)}(q^2) \quad . \tag{5.3.2}$$

The caret over the symbols in Eqs. (5.3.1) and (5.3.2) indicates that we have implemented a model of confinement. For example, in the absence of confinement, $J_{(\omega)}(q^2)$ and $J_{(\rho)}(q^2)$ would be obtained in a calculation of the diagram in Fig 5.1a. Figure 5.1b shows the addition of a ladder of confinement interactions described by a linear potential, $V^C(r) = \kappa r \exp[-\mu r]$. The parameter μ is included to soften the momentum-space singularities of the Fourier transform of $V^C(r)$. (We have used μ = 50 MeV and κ = 0.22 GeV^2 in our calculations.) The ladder of interactions may be summed to define a vertex function [Ce 95a,Ga 96b]. (See the shaded area of Fig 5.1b.) The equation for the vertex is shown in Fig 5.1c. The solution of that equation and the calculation of $\hat{J}_{(\rho)}(q^2)$ and $\hat{J}_{(\omega)}(q^2)$ have been discussed at length in our earlier work [Ce 95a,d]. (Note that, in the absence of isospin symmetry breaking in the Lagrangian, $\hat{J}_{(\omega)}(q^2) = \hat{J}_{(\rho)}(q^2)$.) In Fig 5.2 we show $\hat{J}_{(\rho)}(q^2)$ for both timelike and spacelike values of q^2. The calculation is made in the timelike region using the methods outlined in [Ce 95a]. A cutoff of $\Lambda_3 = 0.702$ GeV is used and the confinement vertex is included with a string tension κ = 0.22 GeV^2. The calculation for the spacelike region is made in a Euclidean momentum space with cutoff Λ_E = 1.0 GeV.

Confinement is neglected for the spacelike region. We find $J_{(\rho)}(0) = 0.0944$ GeV^2 for the calculation made in the spacelike region and $\hat{J}_{(\rho)}(0) = 0.0860$ GeV^2 for the calculation made in the timelike domain. Ideally, the results of the two calculations should overlap near $q^2 = 0$. In Fig 5.2 we have introduced a dotted curve that interpolates between the spacelike and timelike regions.

In the case of the rho meson, we also define a tensor [Ce 95a]

$$\hat{K}^{\mu\nu}_{(\rho)}(q) = -\hat{g}^{\mu\nu}(q)\hat{K}_{(\rho)}(q^2) \quad , \tag{5.3.3}$$

where $\hat{K}^{\mu\nu}_{(\rho)}(q)$ is obtained by evaluating the diagram of Fig 5.3b. The imaginary part of $\hat{K}^{\mu\nu}_{(\rho)}(q)$ arises when both pions go on mass shell, since the introduction of vertex functions associated with the confining potential removes the (unphysical) $q\bar{q}$ cuts that appear in $K^{\mu\nu}_{(\rho)}(q)$. The calculation of ρ-ω mixing requires a small modification of the calculation already made to obtain $\hat{J}^{\mu\nu}_{(\rho)}(q)$ [Ce 95a]. We had

$$-i\hat{J}^{\mu\nu}_{(\rho)}(q) = (-1)n_c n_f \int \frac{d^4k}{(2\pi)^3} \mathrm{Tr}\left[iS(q/2+k)\Gamma^{\mu}(q,k)iS(-q/2+k)\hat{\gamma}^{\nu}\right] \tag{5.3.4}$$

where $\Gamma^{\mu}(q,k)$ is the confining vertex and $\hat{\gamma}^{\nu} \equiv \gamma^{\nu} - \not{q}q^{\nu}/q^2$. Here, $n_f = 2$ is the number of flavors and $n_c = 3$ is the number of colors. We may define a tensor $\hat{J}^{\mu\nu}_{(\rho\omega)}(q)$ by introducing one factor of τ_3 in Eq. (5.3.4) and removing the factor of n_f. More precisely, we can define

$$\hat{J}^{\mu\nu}_{(\rho\omega)}(q) = \frac{1}{n_f}\left[\hat{J}^{\mu\nu}_{(\rho)}(q,m_u) - J^{\mu\nu}_{(\rho)}(q,m_d)\right] \quad , \tag{5.3.5}$$

where m_u and m_d are the constituent masses of the up and down quarks. (Note that $\hat{J}^{\mu\nu}_{(\rho)}(q) = \hat{J}^{\mu\nu}_{(\omega)}(q)$, if $m_u = m_d$.)

Thus, we see that we may use the original calculation made for $\hat{J}^{\mu\nu}_{(\rho)}(q)$ and only consider the variation of that quantity with the constituent quark mass, as in Eq. (5.3.5). [See Fig 5.4] Indeed, the ρ subscripts on the right-hand side of Eq. (5.3.5) could be changed to ω subscripts with any change in $\hat{J}^{\mu\nu}_{(\rho\omega)}(q)$, since we are actually using Eq. (5.3.5) to obtain the difference of an integral involving the up quark and one involving the down quark.

By studying the gap equation of the NJL model, one finds that $m_u - m_d = m_u^0 - m_d^0$, where m_u^0 and m_d^0 are the current quark masses that appear in the Lagrangian. It is again useful to write

$$\hat{J}^{\mu\nu}_{(\rho\omega)}(q) = -\hat{g}^{\mu\nu}(q)\hat{J}_{(\rho\omega)}(q^2) \quad , \tag{5.3.6}$$

and, using Eq. (5.3.5), we see that

$$\hat{J}_{(\rho\omega)}(q^2) = \frac{1}{n_f}\left[\hat{J}_{(\rho)}(q^2, m_u) - \hat{J}_{(\rho)}(q^2, m_d)\right] \quad . \tag{5.3.7}$$

Note that $\hat{J}_{(\rho\omega)}(q^2)$ is positive for $q^2 > 0$, since $\hat{J}_{(\rho)}(q^2, m)$ is a decreasing function of m and $m_d > m_u$. (For example, we show $\hat{J}_{(\rho)}(q^2, m)$ as a function of m in Fig 5.4 for several values of q^2.) Note that, since $\hat{K}_{(\rho)}(q^2)$ is small, we do not concern ourselves with isospin symmetry violations ($m_d \neq m_u$) in the calculation of $\hat{K}_{(\rho)}(q^2)$.

At this point we may proceed with a diagrammatic analysis. For example, in Fig 5.5a we show $\hat{J}_{(\rho\omega)}(q^2)$, where the cross-hatching reminds us that this diagram is nonzero due to the isospin violation. The calculation of the current correlator requires that we sum the additional diagrams shown in Fig 5.5b, where we have included only a single factor of $\hat{J}_{(\rho\omega)}(q^2)$ in each diagram, since that quantity is quite small. In

evaluating these diagrams it is useful to note that

$$\hat{g}^{\mu\alpha}(q)\,\hat{g}_{\alpha}{}^{\nu}(q) = \hat{g}^{\mu\nu}(q) \quad . \tag{5.3.8}$$

The result for the correlator may be improved upon by including factors of $\hat{K}_{(\rho)}(q^2)$ and $\hat{K}_{(\omega)}(q^2)$. We find that the diagrammatic analysis leads to the relation

$$\frac{\tilde{\theta}_3(q^2)}{\left[q^2 - \left[m_\rho - \frac{i\Gamma_\rho}{2}\right]^2\right]\left[q^2 - \left[m_\omega - \frac{i\Gamma_\omega}{2}\right]^2\right]} \tag{5.3.9}$$

$$= -\frac{1}{1 - G_\rho\left[\hat{J}_{(\rho)}(q^2) + \hat{K}_{(\rho)}(q^2)\right]}\hat{J}_{(\rho\omega)}(q^2)\frac{1}{1 - G_\omega\left[\hat{J}_{(\omega)}(q^2) + \hat{K}_{(\omega)}(q^2)\right]}$$

We have noted that $\hat{J}_{(\rho\omega)}(q^2)$ is positive for $q^2 > 0$, so that $\tilde{\theta}_3(q^2)$ is negative in that region.

In order to extract an expression for $\tilde{\theta}_3(q^2)$ from Eq. (5.3.9), it is useful to use a momentum-space bosonization procedure with the aim of exhibiting the complex zeroes of the denominators on the right-hand side of Eq. (5.3.9) [Be 92]. As a first step, we separate $\hat{K}_{(\rho)}(q^2)$ and $\hat{K}_{(\omega)}(q^2)$ into real and imaginary parts. We have seen in a recent work [Ga 96b] that the following representation is useful for $q^2 > 0$,

$$\hat{J}_{(\rho)}(q^2) + \mathrm{Re}\,\hat{K}_{(\rho)}(q^2) = r_1 - \frac{r_2}{q^2 - \tilde{m}_\rho^2} \quad , \tag{5.3.10}$$

where r_1, r_2, and $\tilde{m}_\rho$ are parameters. We will provide a similar representation for the isoscalar channel, but we will drop Re $\hat{K}_{(\omega)}(q^2)$, since it is very small. Thus, we put

For example, in the absence of $\hat{K}_{(\omega)}(q^2)$, we find

$$\hat{J}_{(\omega)}(q^2) = v_1 - \frac{v_2}{q^2 - \tilde{m}_\omega^2} \quad . \tag{5.3.11}$$

$$\frac{1}{1 - G_\omega \hat{J}_{(\omega)}(q^2)} = - \frac{g^2_{\omega qq}(q^2)}{q^2 - m_\omega^2} \frac{1}{G_\omega} \quad , \tag{5.3.12}$$

with

$$m_\omega^2 = \tilde{m}_\omega^2 - \frac{v_2}{G_\omega^{-1} - v_1} \quad , \tag{5.3.13}$$

and

$$g^2_{\omega qq}(q^2) = \frac{\tilde{m}_\omega^2 - q^2}{G_\omega^{-1} - v_1} \quad . \tag{5.3.14}$$

[See Table 5.1.] The expressions for m_ρ^2 and $g^2_{\rho qq}(q^2)$ are analogous to those in Eqs. (5.3.13) and (5.3.14), with G_ω, v_1 and v_2 replaced by G_ρ, r_1 and r_2. Note that $\tilde{m}_\omega^2 > q^2$ in this representation.

The momentum-dependent coupling constant, $g^2_{\omega qq}(q^2)$, appears naturally in this analysis. For nuclear structure studies the relevant value of the coupling constant is $g^2_{\omega qq}(0)$, since such studies are performed for relatively small, spacelike values of q^2. (The representation given in Eqs. (5.3.10) and (5.3.11) may also be used for small spacelike values of q^2. For timelike values, we have the restriction $q^2 < \tilde{m}_\omega^2$ or $q^2 < \tilde{m}_\rho^2$.)

In the case of the rho, we keep Re $\hat{K}_{(\rho)}(q^2)$ and Im $\hat{K}_{(\rho)}(q^2)$ and find, upon use of Eq. (5.3.10), that

$$\frac{1}{1 - G_\rho \left\{ [\hat{J}_{(\rho)}(q^2) + \mathrm{Re}\hat{K}_{(\rho)}(q^2)] + i\,\mathrm{Im}\hat{K}_{(\rho)}(q^2) \right\}}$$

$$= - \frac{g^2_{\rho qq}(q^2) G_\rho^{-1}}{q^2 - m_\rho^2 - i \frac{(q^2 - \tilde{m}_\rho^2)}{G_\rho^{-1} - r_1} \mathrm{Im}\hat{K}_{(\rho)}(q^2)} \tag{5.3.15}$$

$$\simeq - \frac{g^2_{\rho qq}(q^2)\, G_\rho^{-1}}{q^2 - \left[m_\rho - i \frac{\Gamma_\rho(q^2)}{2} \right]^2} \quad . \tag{5.3.16}$$

We may obtain an expression for $\Gamma_\rho(q^2)$ by comparing Eqs. (5.3.16) and (5.3.15), if we neglect $\Gamma_\rho^2(q^2)$. Alternatively we may use Eq. (5.3.15), which provides more accurate representation of the result of our analysis.

Finally, we have, upon use of Eq. (5.3.9),

$$\tilde{\theta}_3(q^2) = - g^2_{\rho qq}(q^2) \frac{\hat{J}_{(\rho\omega)}(q^2)}{G_\rho G_\omega} g^2_{\omega qq}(q^2) \quad , \tag{5.3.17}$$

and

$$\theta_3(q^2) = - \frac{g^\omega g^\rho}{12 m_\omega^2 m_\rho^2} g^2_{\rho qq}(q^2) \frac{\hat{J}_{(\rho\omega)}(q^2)}{G_\rho G_\omega} g^2_{\omega qq}(q^2) \quad . \tag{5.3.18}$$

To carry out the calculation, we need the following parameters [Ga 96b]:

$G_\rho = 7.12\ \text{GeV}^{-2}$, $r_1 = 0.0304\ \text{GeV}^2$, $r_2 = 0.0968\ \text{GeV}^4$, $\bar{m}_\rho^2 = \bar{m}_\omega^2 = 1.476\ \text{GeV}^2$, $G_\omega = 7.86\ \text{GeV}^{-2}$, $v_1 = 0.0284\ \text{GeV}^2$, and $v_2 = 0.0850\ \text{GeV}^4$.

We also use the empirical values, $g^\omega = 15.2$ and $g^\rho = 5.3$ [Du 83], while [Ha 94, Iq 95] has $g^\omega = 3g^\rho$ and $(g^\rho)^2/4\pi = 2.4$.

Considering the on-shell value, $q^2 = m_\omega^2$, we find $\hat{J}_{(\rho\omega)}(m_\omega^2) = 4.03 \times 10^{-4}\ \text{GeV}^2$, if $m_d = 262$ MeV and $m_u = 260$ MeV. (See Fig 5.6.) Using the various parameters given above, we then calculate $\bar{\theta}_3(m_\omega^2) = -0.493 \times 10^{-3}\ \text{GeV}^6$ and, from Eq. (5.3.18), we find $\theta_3(m_\omega^2) = (18.47\ \text{GeV}^{-4})\ \bar{\theta}(m_\omega^2) = -9106\ \text{MeV}^2$. Note that, if $m_d^0 - m_u^0 = 3.0$ MeV, we have $\theta_3(m_\omega^2) = -13{,}660\ \text{MeV}^2$.

It is of interest to ask for the relation between $\theta_3(m_\omega^2)$ and $<\rho\,|\,H_{SB}\,|\,\omega>$. In reference listed in [Mc 75], $<\rho\,|\,H_{SB}\,|\,\omega>$ was defined in terms of the ratio of the width for two-pion decay of the omega to the width of the rho:

$$\frac{\Gamma_{\omega\to 2\pi}}{\Gamma_\rho} = \left[\frac{<\rho\,|\,H_{SB}\,|\,\omega>}{m_\rho \Gamma_\rho}\right]^2 . \qquad (5.3.19)$$

From this relation, it was found that $<\rho\,|\,H_{SB}\,|\,\omega> = -(4520 \pm 600)\ \text{MeV}^2$, a value quoted in the recent literature.

Now, we note that, from Eqs. (5.3.15) and the analog of Eq. (5.3.14) for the rho meson, we have

$$\Gamma_\rho = \frac{g^2_{\rho qq}(m^2_\rho)}{m_\rho} \operatorname{Im} \hat{K}_{(\rho)}(m^2_\rho) \quad . \tag{5.3.20}$$

In a similar fashion, we find

$$\Gamma_{\omega\to 2\pi} = \frac{g^2_{\omega qq}(m^2_\omega)}{m_\omega} \operatorname{Im} \hat{K}_{(\omega)}(m^2_\omega) \quad . \tag{5.3.21}$$

Further, we see that Im $\hat{K}_{(\omega)}(m^2_\omega)$ contains Im $\hat{K}_{(\rho)}(m^2_\omega)$ as a factor in a ρ-ω mixing calculation of the width of the omega. We find

$$\frac{\Gamma_{\omega\to 2\pi}}{\Gamma_\rho} = \left[\frac{g^2_{\rho qq}(m^2_\omega) J_{(\rho\omega)}(m^2_\omega)}{m_\rho \Gamma_\rho}\left[\frac{g_{\omega qq}(m^2_\omega)}{g_{\rho qq}(m^2_\rho)}\right]\right]^2 \left[\frac{m_\omega}{m_\rho}\right] \tag{5.3.22}$$

where we have used the fact that a consideration of the relevant phase space gives $\operatorname{Im} \hat{K}_{(\rho)}(m^2_\omega) / \operatorname{Im} \hat{K}_{(\rho)}(m^2_\rho) \simeq (m^2_\omega / m^2_\rho)$. In writing Eq. (5.3.22), we have neglected <u>direct</u> $\omega \to \pi^+ + \pi^-$ decay and taken the decay to proceed via ω-ρ mixing, as noted above.

We see upon using Eq. (5.3.19), that

$$< \rho \mid H_{SB} \mid \omega > \; = \; - g^2_{\rho qq}(m^2_\omega) \hat{J}_{(\rho\omega)}(m^2_\omega) \left[\frac{g_{\omega qq}(m^2_\omega)}{g_{\rho qq}(m^2_\rho)}\right] \quad , \tag{5.3.23}$$

where we have replaced $(m_\omega / m_\rho)^{1/2} \simeq 1.01$ by 1. The last factor in Eq. (5.3.23) is equal to 1.056, while $g_{\rho qq}(m^2_\omega) = 2.81$. We recall that $\hat{J}_{(\rho\omega)}(q^2)$ is proportional to $m^0_d - m^0_u$. If we put $m^0_d - m^0_u = 2.69$, we have $\hat{J}_{(\rho\omega)}(m^2_\omega) = 5.42 \times 10^{-4}$ GeV^2 and, therefore $< \rho \mid H_{SB} \mid \omega > \; = -4520$ MeV^2.

Returning to Eq. (5.3.18), we see that, with our treatment of the ρ and ω fields,

$$\theta_3(m_\omega^2) = \frac{g^\omega g^\rho}{12 m_\rho^2 m_\omega^2} \frac{g_{\omega qq}(m_\omega^2) g_{\rho qq}(m_\rho^2)}{G_\rho G_\omega} < \rho \mid H_{SB} \mid \omega > \qquad (5.3.24)$$

$$\simeq 2.74 < \rho \mid H_{SB} \mid \omega > \qquad (5.3.25)$$

where we have used $G_\rho = 7.12$ GeV^{-2}, $G_\omega = 7.86$ GeV^{-2}, $g^\rho = 5.3$, $g^\omega = 15.2$, $g_{\omega qq}(m_\omega^2) = 2.95$ and $g_{\rho qq}(m_\rho^2) = 2.81$. (See Table 5.1.) Our result for $\theta_3(m_\omega^2)$ is based upon the use of Eq. (5.3.19) to define $< \rho \mid H_{SB} \mid \omega >$, as in [Mc 75]. It is in that reference that the value $< \rho \mid H_{SB} \mid \omega > = -(4520 \pm 600)$ MeV^2 is extracted from the data.

In this section we have used the empirical values for g^ρ and g^ω. In the next section we discuss the values obtained for g^ρ and g^ω in our extended NJL model.

5.4. Relation of Meson Decay Constants and the Bosonization Scheme

In the simplest bosonization scheme [Be 92], the source of the rho and the omega fields are vector currents introduced previously,

$$(q^2 - m_\omega^2)\omega^\mu(x) = -g_{\omega qq}\bar{q}(x)\gamma^\mu q(x) \tag{5.4.1}$$

and

$$(q^2 - m_\rho^2)\rho^\mu(x) = -g_{\rho qq}\bar{q}(x)\gamma^\mu \tau_3 q(x) \quad . \tag{5.4.2}$$

It is then useful to introduce the currents of Eqs. (5.2.5) and (5.2.6), so that Eqs. (5.4.1) and (5.4.2) become

$$(q^2 - m_\omega^2)\omega^\mu(x) = -6g_{\omega qq} j_S^\mu(x) \tag{5.4.3}$$

and

$$(q^2 - m_\rho^2)\rho^\mu(x) = -2g_{\omega qq} j_V^\mu(x) \quad . \tag{5.4.4}$$

Since the decay constants are calculated for on-mass-shell mesons, we have

$$g^\omega = 6g_{\omega qq}(m_\omega^2) \quad , \tag{5.4.5}$$

$$g^\rho = 2g_{\rho qq}(m_\rho^2) \quad , \tag{5.4.6}$$

where we expect that $g^\rho \simeq 3g^\omega$. Equations (5.4.5) and (5.4.6) are mean-field results for a theory without confinement. We will not make use of Eqs. (5.4.5) and (5.4.6). However, with $g_{\omega qq}(m_\omega^2) = 2.95$ and $g_{\rho qq}(m_\rho^2) = 2.83$, we have $g^\omega = 17.7$ and $g^\rho = 5.66$, which compare favorably with the empirical values $g^\omega = 15.2$ and $g^\rho = 5.3$.

We may calculate g^ρ and g^ω using the extended NJL model. We find

$$g^{\rho} = \frac{2m_{\rho}^2}{g_{\rho qq}(m_{\rho}^2)\,[\hat{J}_{(\rho)}(m_{\rho}^2) + \mathrm{Re}\,\hat{K}_{(\rho)}(m_{\rho}^2)]} \quad , \tag{5.4.7}$$

$$= \frac{2m_{\rho}^2 G_{\rho}}{g_{\rho qq}(m_{\rho}^2)}, \tag{5.4.8}$$

and

$$g^{\omega} = \frac{6m_{\omega}^2}{g_{\omega qq}(m_{\omega}^2)\,\hat{J}_{(\omega)}(m_{\omega}^2)} \quad , \tag{5.4.9}$$

$$= \frac{6m_{\omega}^2 G_{\omega}}{g_{\omega qq}(m_{\omega}^2)} \quad . \tag{5.4.10}$$

Using $g_{\rho qq}(m_{\rho}^2) = 2.81$, $g_{\omega qq}(m_{\omega}^2) = 2.95$ (see Table 5.1), $G_{\omega} = 7.86\ \mathrm{GeV}^{-2}$, and $\hat{J}_{(\rho)}(m_{\rho}^2) + \mathrm{Re}\,\hat{K}_{(\rho)}(m_{\rho}^2) = 0.140\ \mathrm{GeV}^2$, we find $g^{\rho} = 3.01$ and $g^{\omega} = 9.80$. These numbers may be compared to the empirical values, $g^{\rho} = 5.3$ and $g^{\omega} = 15.2$. Since our calculated value of g^{ρ} and g^{ω} are too small, we see a need for further exploration of the parameter space of our NJL model. (It is interesting to note that the calculations reported in [Kl 90] gave $g^{\rho} = 7.0$ and $g^{\omega} = 24.0$, which are larger than the empirical values quoted above. Note that in [Kl 90] the notation for the decay constants differs from that used here.)

We note that to obtain values of $\theta_3(q^2)$ for spacelike q^2, it is best to return to Eq. (5.3.9) and to calculate the various functions that appear on the right-hand side. To obtain $J_{(\rho)}(q^2)$ and $J_{(\omega)}(q^2)$, we may use the expressions given in the Appendix.

One often defines a rho decay constant called f_ρ [Ce 95a]. The relation to g^ρ is

$$f_\rho = \frac{m_\rho}{g^\rho} \quad . \tag{5.4.11}$$

If we use our calculated value of $g^\rho = 3.01$, we find $f_\rho = 0.256$ GeV, which is larger than the empirical value $f_\rho \simeq 0.152$ GeV. (The calculations of isovector current correlators reported in [Ce 95a] used rather different values of m_q and G_ρ than those used in the present work. In [Ce 95a] we found $f_\rho = 0.166$ GeV.)

We may note that the values we have found in [Ga 96b], $g_{\omega qq}(0) = 3.86$ and $g_{\rho qq}(0) = 3.66$, lead to the following consequences, when we consider the one boson-exchange (OBE) model of the nucleon-nucleon interaction [Ma 89]. For omega exchange, $g_{\omega qq}(0) = 3.86$ leads to $g^2_{\omega NN}/4\pi = 20.2$, while the phenomenological value is $g^2_{\omega NN}/4\pi = 20.0$ [Ma 89]. In the model of [Ga 96b], the vector and tensor parts of the rho-nucleon interaction are related by $f_\rho/g_\rho = 3.70$, instead of the phenomenological value of $f_\rho/g_\rho = 6.1$. (The f_ρ of this paragraph should not be confused with f_ρ of Eq. (5.4.11).) However, with $g_{\rho qq}(0) = 3.66$, we found $f_\rho = 20.6$, while $f_\rho^{OBE} = 21.5$ [Ma 89].

5.5. Subtractions for the Correlator

One can argue that, if $\Pi^{(\rho\omega)}(q^2)$, $\Pi^{(\rho)}(q^2)$ and $\Pi^{(\omega)}(q^2)$ are unequal to zero for $q^2 = 0$, one would generate a mass for the photon. Actually, the condition $\Pi^{(\rho\omega)}(0) = 0$ arises on more general grounds [Ma 95,Oc 94]. To implement that constraint, we define a subtracted tensor

$$\bar{\Pi}^{(\rho\omega)}_{\mu\nu}(q) = \hat{g}_{\mu\nu}(q) \frac{\theta_3(q^2)}{\left[q^2 - \left[m_\rho - \frac{i\Gamma_\rho}{2}\right]^2\right]\left[q^2 - \left[m_\omega - \frac{i\Gamma_\omega}{2}\right]^2\right]} - \frac{\theta_3(0)}{m_\rho^2 m_\omega^2} \quad (5.5.1)$$

$$= \hat{g}_{\mu\nu}(q) \frac{\bar{\theta}_3(q^2)}{\left[q^2 - \left[m_\rho - \frac{i\Gamma_\rho}{2}\right]^2\right]\left[q^2 - \left[m_\omega - \frac{i\Gamma_\omega}{2}\right]^2\right]} , \quad (5.5.2)$$

so that

$$\bar{\theta}_3(q^2) = \theta_3(q^2) - \left[q^2 - \left[m_\rho - \frac{i\Gamma_\rho}{2}\right]^2\right]\left[q^2 - \left[m_\omega - \frac{i\Gamma_\omega}{2}\right]^2\right] \frac{\theta_3(0)}{m_\rho^2 m_\omega^2} \quad (5.5.3)$$

Note that $\bar{\theta}_3(0) = 0$, as desired. We remark that, if we evaluate $\bar{\theta}_3(q^2)$ at $q^2 = (m_\omega - i\Gamma_\omega/2)^2$, we find

$$\bar{\theta}_3(m_\omega^2) = \theta_3(m_\omega^2) \quad . \quad (5.5.4)$$

Therefore, our results for $\theta_3(m_\omega^2)$ pertain to $\bar{\theta}_3(m_\omega^2)$ as well. (See Fig. 5.7.)

5.6. Current Quark Difference

In this work we have shown how the NJL model, extended to include a description of confinement [Ce 95a,d], may be used to calculate the mixed-current correlator, which is nonzero due to explicit isospin symmetry breaking in the Lagrangian of the model. (In previous works, we have shown how our methods may be used to calculate correlators of the scalar-isoscalar current, $j_s(x) = \bar{q}(x)q(x)$ [Ce 95c] and the correlator of the vector-isovector current [Ce 95a].) In the present study, we obtain the experimental value of $< \rho \mid H_{SB} \mid \omega > = -(4520 \pm 600)$ MeV^2, if $m_d^0 - m_u^0 = 2.69$ MeV. Taking the errors for $< \rho \mid H_{SB} \mid \omega >$ into account, we suggest that $m_d^0 - m_u^0 = 2.7 \pm 0.3$ MeV. From [Ga 82] we have $m_u^0 = 5 \pm 2$ MeV and $m_d^0 = 9 \pm 3$ MeV. These values are consistent with $m_{avg}^0 = 5.5$ MeV, $m_d = 6.85$ MeV, and $m_u = 4.15$ MeV. For that choice, $m_d^0 - m_u^0 = 2.70$ MeV, which was the value given above. However, values of $m_d^0 - m_u^0$ anywhere in the range of 1 to 5 MeV are also consistent with the uncertainties in the values of m_u^0 and m_d^0. (We remark that $m_{avg}^0 = 5.5$ MeV yields the correct pion mass, when $\Lambda_E = 1.0$ GeV [Ca 92].) Clearly, more information concerning the value of $m_d^0 - m_u^0$ would be quite useful in evaluating the success of our calculation.

Finally, we note that a recent analysis [Oc 95] yields $< \rho \mid H_{SB} \mid \omega > = -(3800 \pm 370)$ MeV^2. If we accept that value we would have $m_d^0 - m_u^0 = 2.26 \pm 0.23$ MeV, which is smaller than the value given above.

Chapter 6. Gauge Invariance and Confinement in a Generalized NJL Model

6.1. Subtraction Procedure for the NJL Model

In the application of the Nambu−Jona-Lasinio model to the study of hadron structure one calculates quark-antiquark loop diagrams of the type shown in Fig. 1 [Vo 92,Kl 92]. In this work we will concentrate on those diagrams that appear when the $q\bar{q}$ system has the quantum numbers $J = 1^-$, with isospin 0 or 1. These diagrams arise in the study of the omega and rho mesons when using the NJL model. For such studies it is important to include a model of confinement. We have shown how that may be done in an earlier work [Ce 95a]. For example, if we include a ladder of confining interactions, as shown in Fig. 6.1b, we may define polarization tensors that do not have the unitarity cuts that would have appeared, in the absence of confinement, if both the quark and antiquark go on mass shell [Ce 95b].

With reference to Fig. 6.1a, we define a tensor [Ce 95a]

$$-iJ^{\mu\nu}(q) = (-1)n_c n_f \mathrm{Tr}\int \frac{d^4k}{(2\pi)^4}\left[\gamma^\mu iS(k)\gamma^\nu iS(k+q)\right] , \qquad (6.1.1)$$

where $n_c = 3$ is the number of colors and $n_f = 2$ is the number of flavors. Further, $S(k) = [\not{k} - m + i\epsilon]^{-1}$, where m is the constituent quark mass. Often the integral of Eq. (6.1.1) is regulated by including a cutoff, Λ_E. After pass to a Euclidean momentum space, one imposes the condition $k_E^2 < \Lambda_E^2$ [Vo 92,Kl 92]. (Typically, $\Lambda_E \sim 1$ GeV is used.) That kind of regularization destroys the gauge invariance of the result.

Therefore, the following scheme has been adopted [Vo 92,Kl 92]. In Eq. (6.1.1), γ^μ is replaced by $\hat{\gamma}^\mu = \gamma^\mu - \not{q} q^\mu / q^2$ and γ^μ is replaced by $\hat{\gamma}^\nu = \gamma^\nu - \not{q} q^\nu / q^2$. This allows one to write

$$J^{\mu\nu}(q) = -\bar{g}^{\mu\nu}(q) J(q^2) \quad , \tag{6.1.2}$$

where

$$\bar{g}^{\mu\nu}(q) = g^{\mu\nu} - q^\mu q^\nu / q^2 \quad . \tag{6.1.3}$$

This procedure imposes the condition $q_\mu J^{\mu\nu}(q) = J^{\mu\nu}(q) q_\nu = 0$. However, we must also have $J(0) = 0$ to avoid generating a mass for the photon [Fr 95.Oc 94]. That may be accomplished by making a subtraction, so that $J(q^2)$ is replaced by $J(q^2) - J(0)$. This is the procedure used by Weise and collaborators in their extensive applications of the NJL model to the study of hadron structure [Vo 92,Kl 92]. (Note that, in their work, it was necessary to neglect $\mathrm{Im} J(q^2)$, since those authors did not include a model of confinement.) One may avoid making a subtraction by using a regularization scheme that respects gauge invariance. For example, Friedrich and Reinhardt use a proper-time regularization scheme and obtain vacuum polarization diagrams of the correct structure in their study of rho-omega mixing [Fr 95]. (A more complete discussion of this matter may be found in [Oc 94].)

In our work dealing with confinement, we have used a Euclidean momentum-space cutoff for spacelike $q^2 (q^2 < 0)$ and a cutoff for each of the three-momenta in the loop integrals, when $q^2 > 0$ [Ce 95a]. The (Minkowski-space) cutoff, Λ_3, used for $q^2 > 0$, was chosen so that the vacuum polarization integrals calculated for q^2 and

$q^2 < 0$ were (approximately) continuous at $q^2 = 0$. (See Fig. 6.2.) In our earlier work, we calculated the tensor

$$-i\hat{J}^{\mu\nu}(q) = n_c n_f \mathrm{Tr} \int \frac{d^4k}{(2\pi)^4} \left[\hat{\Gamma}^{\mu}(q, k)\, S(k)\, \hat{\gamma}^{\nu}\, S(k+q) \right] , \qquad (6.1.4)$$

where $\hat{\Gamma}^{\mu}(q, k)$ was the vertex function that arose when we summed a ladder of confining interactions [Ce 95a,c]. Our calculation was made such that $q_{\mu} \hat{\Gamma}^{\mu}(q, k) = 0$. Thus, we could define

$$\hat{J}^{\mu\nu}(q) = -\tilde{g}^{\mu\nu}(q) \hat{J}(q^2) . \qquad (6.1.5)$$

In the limit that the current masses of the up and down quarks are equal, the tensors, $\hat{J}^{\mu\nu}(q)$, calculated for the rho and omega mesons are the same. Therefore, we can identify $\hat{J}_{(\rho)}(q^2) = \hat{J}_{(\omega)}(q^2) = \hat{J}(q^2)$. In Fig. 6.2, we show value of $\hat{J}_{(\rho)}(q^2)$ calculated in [Ga 96b]. (The dotted line in the figure interpolates between the calculations made for $q^2 > 0$ and $q^2 < 0$ to yield a continuous curve.) In Fig. 6.2, we see that $\hat{J}_{(\rho)}(0) \neq 0$. We may make a subtraction to obtain $\hat{J}_{(\rho)}(0) = 0$, as discussed above. This subtraction does not change the momentum-space bosonization we have used in our work. For example, we may define a T matrix in the omega channel,

$$T_{\omega}(q^2) = \frac{G_{\omega}}{1 - G_{\omega} \hat{J}_{(\omega)}(q^2)} , \qquad (6.1.6)$$

where we have neglected reference to the Dirac and isospin matrices, for simplicity. (In Eq. (6.1.6), we have summed a string of $q\bar{q}$ loop integrals. The simplicity of the NJL model allows us to provide a simple result for that sum.) In Eq. (6.1.6) G_{ω} is a parameter of the Lagrangian of our extended NJL model,

$$\mathcal{L}(x) = \bar{q}(x)\left(i\partial - m_q^0\right)q(x) - \frac{G_S}{2}\left[\left(\bar{q}(x)q(x)\right)^2 + \left(\bar{q}(x)i\gamma_5\vec{\tau}q(x)\right)^2\right]$$

$$- \frac{G_V}{2}\left[\left(\bar{q}(x)\gamma^\mu\vec{\tau}q(x)\right)^2 + \left(\bar{q}(x)\gamma_5\gamma^\mu\vec{\tau}q(x)\right)^2\right] \qquad (6.1.7)$$

$$- \frac{G_\omega}{2}\,\bar{q}(x)\gamma^\mu q(x) + \mathcal{L}_{conf}(x) \quad .$$

Here, $\mathcal{L}_{conf}(x)$ refers to the model of confinement that we have introduced [Ce 95a,c]. In a momentum-space bosonization scheme, we may put [Be 92]

$$\frac{G_\omega}{1 - G_\omega \hat{J}_{(\omega)}(q^2)} = -\frac{g^2_{\omega qq}(q^2)}{q^2 - m_\omega^2} \quad . \qquad (6.1.8)$$

Equation (6.1.8) serves as a definition of the momentum-dependent coupling constant $g_{\omega qq}(q^2)$. (The widths of the omega and rho mesons may also be considered. However, we do not enter into that discussion here.) We now consider the subtraction procedure, replacing $\hat{J}_{(\omega)}(q^2)$ by $\hat{J}_{(\omega)}(q^2) - \hat{J}_{(\omega)}(0)$, for example. If we simultaneously replace G_ω^{-1} by $\bar{G}_\omega^{-1} \equiv G_\omega^{-1} - \hat{J}_{(\omega)}(0)$, we see that $g^2_{\omega qq}(q^2)$ and m_ω^2 are unchanged. (On the other hand, replacing G_ω by $\bar{G}_\omega$ does significantly increase the (dimensionless) meson decay constant, g^ω, that has an empirical value of about 15.2 [Sh 97b].)

In the present work, we wish to investigate the merits of the subtraction procedure, while maintaining our model of confinement. To that end, we will introduce a regularization procedure (Pauli-Villars) that respects gauge invariance and show how our model of confinement may be implemented in this case. That analysis is carried out in Section 6.2. In Section 6.3 we provide further details concerning our model of confinement, while Section 6.4 provides some additional discussion.

6.2. Gauge Invariance and Confinement in an Extended NJL Model

First, let us consider the calculation of the vacuum polarization tensor in QED. We will follow the discussion of Kaku [Ka 95]. Kaku defines the tensor

$$\Pi_{\mu\nu,m}(q) = -e^2 \mathrm{Tr} \int \frac{d^4k}{(2\pi)^4} \gamma_\mu \frac{1}{\not k - m + i\epsilon} \gamma_\nu \frac{1}{\not k - m + i\epsilon} \quad , \tag{6.2.1}$$

where the dependence on the fermion mass is made explicit. He then defines

$$\tilde{\Pi}_{\mu\nu}(q) = \Pi_{\mu\nu,m}(q) - \Pi_{\mu\nu,M}(q) \quad , \tag{6.2.2}$$

where M is the Pauli-Villars regulator mass. Further, we have the definition

$$\tilde{\Pi}_{\mu\nu}(q) = (g_{\mu\nu}q^2 - q_\mu q_\nu)\,\tilde{\Pi}_1(q^2) \quad . \tag{6.2.3}$$

The result obtained for $\tilde{\Pi}_1(q^2)$ is

$$\tilde{\Pi}_1(q^2) = \frac{ie^2}{12\pi^2}\left\{C + 2\left[1 + \frac{2m^2}{q^2}\right]\left[\left[\frac{4m^2 - 1}{q^2}\right]^{1/2} \cot^{-1}\left[\frac{4m^2}{q^2} - 1\right]^{1/2} - 1\right]\right\} \quad , \tag{6.2.4}$$

for $0 < q^2 < 4m^2$.

Now let us assume that we regulate $J(q^2)$ of Eq. (6.1.1) using the Pauli-Villars method. We may call the result $\tilde{J}(q^2) = J_m(q^2) - J_M(q^2)$. The relation between $\tilde{J}(q^2)$ and $\tilde{\Pi}_1(q^2)$ is then

$$\tilde{J}(q^2) = i\frac{n_c n_f}{e^2} q^2 \tilde{\Pi}_1(q^2) \quad . \tag{6.2.5}$$

At this point we have not introduced the effect of confinement. (Note that the condition

$\bar{J}(q^2) = 0$ corresponds to the requirement that $\bar{\Pi}_1(q^2)$ not have a simple pole at $q^2 = 0$.)

Equations (6.2.4) and (6.2.5) yield a result for $\bar{J}(q^2)$ valid in the region $0 < q^2 < 4m^2$,

$$\bar{J}(q^2) = -\frac{n_c n_f}{12\pi^2} q^2 \left\{ C + 2\left[1 + \frac{2m^2}{q^2}\right]\left[\left[\frac{4m^2 - 1}{q^2}\right]^{1/2} \cot^{-1}\left[\frac{4m^2}{q^2} - 1\right]^{1/2} - 1\right]\right\} , \tag{6.2.6}$$

with $\bar{J}(0) = 0$, as expected.

In the case that $q^2 > 4m^2$, we may introduce

$$x = \left[1 - \frac{4m^2}{q^2}\right]^{1/2} , \tag{6.2.7}$$

and obtain

$$\mathrm{Re}\,\bar{J}(q^2) = -\frac{n_c n_f}{12\pi^2} q^2 \left\{ C + 2\left[1 + \frac{2m^2}{q^2}\right]\left[\frac{x}{2} \ln\left[\frac{1+x}{1-x}\right] - 1\right]\right\} , \tag{6.2.8}$$

and

$$\mathrm{Im}\,\bar{J}(q^2) = \frac{n_c n_f}{12\pi} q^2 \left[1 + \frac{2m^2}{q^2}\right]\left[1 - \frac{4m^2}{q^2}\right]^{1/2} . \tag{6.2.9}$$

(In Eq. (6.2.8), $x < 1$.)

For $q^2 \leq 0$, we may define

$$y = \left[1 + \frac{4m^2}{|q^2|}\right]^{1/2} \tag{6.2.10}$$

and write

$$\tilde{J}(q^2) = -\frac{n_c n_f}{12\pi^2} q^2 \left\{ -\ln\left[\frac{M^2}{m^2}\right] + \frac{1}{3} + 2\left[1 + \frac{2m^2}{q^2}\right]\left[\frac{y}{2}\ln\left[\frac{y+1}{y-1}\right] - 1\right]\right\}. \tag{6.2.11}$$

From Eq. (6.2.10), we see that $y \geq 1$. We note that

$$\tilde{\Pi}_1(0) = \frac{ie^2}{12\pi^2}\left[-\ln\frac{M^2}{m^2}\right] . \tag{6.2.12}$$

(In QED, the dependence on $\ln(M^2/m^2)$ is removed when introducing the renormalized charge. The NJL model is not renormalizable and the various observables depend upon the regulator mass.)

We now want to show how these results are modified when we introduce confinement. In particular, our model of confinement will make the polarization tensor real for $q^2 < 4M^2$.

6.3. Numerical Results

It is useful to introduce the notation $\hat{J}_m^{\mu\nu}(q)$ for the tensor defined in Eq. (6.1.4). Recall that m is the constituent quark mass. (Note that we may replace $\hat{\gamma}^\mu$ by γ^μ, if we are using a regularization scheme that preserves gauge invariance.) Let us define

$$\bar{J}^{\mu\nu}(q) = \hat{J}_m^{\mu\nu}(q) - J_M^{\mu\nu}(q) \quad , \tag{6.3.1}$$

where $J_M^{\mu\nu}(q)$ is obtained from Eq. (6.1.1) upon replacing m by M. (This tensor is depicted in a schematic fashion in Fig. 6.3a.) Note that we do not include confinement in the calculation of $J_M^{\mu\nu}(q)$.

It is useful to rewrite Eq. (6.3.1)

$$\bar{J}^{\mu\nu}(q) = \left[J_m^{\mu\nu}(q) - J_M^{\mu\nu}(q)\right] + \left[\hat{J}_m^{\mu\nu}(q) - J_m^{\mu\nu}(q)\right] \quad , \tag{6.3.2}$$

where we have added and subtracted $J_m^{\mu\nu}(q)$. It is also useful to define

$$\bar{J}^{\mu\nu}(q) = -\bar{g}^{\mu\nu}(q)\,\bar{J}(q^2) \quad . \tag{6.3.3}$$

For completeness, we also write

$$\tilde{J}^{\mu\nu}(q) = J_m^{\mu\nu}(q) - J_M^{\mu\nu}(q) \quad , \tag{6.3.4}$$

$$= -\tilde{g}^{\mu\nu}(q)\,\tilde{J}(q^2) \quad . \tag{6.3.5}$$

The value of $\tilde{J}(q^2)$ was given in Eqs. (6.2.5)-(6.2.9), where we gave the results for the Pauli-Villars regularization procedure, without reference to confinement. The second bracketed term of Eq. (6.3.2) may be written as [Ce 95a]

$$-i\left[\hat{J}_m^{\mu\nu}(q) - J_m^{\mu\nu}(q)\right] = (-1)n_c n_f \mathrm{Tr}\int \frac{d^4k}{(2\pi)^4}\left[(\Gamma^\mu(q,k) - \gamma^\mu) iS_m(k)\gamma^\nu iS_m(q+k)\right] \ ,$$

(6.3.4)

where $S_m(k) = [\not{k} - m + i\epsilon]^{-1}$. The contributions to the integral in Eq. (6.3.4) are finite only in a limited region, since $\Gamma^\mu(q,k) \to \gamma^\mu$ (in the frame where $\vec{q} = 0$), if $|\vec{k}|$ is large. To see this in more detail, let us consider some results of [Ce 95a], obtained by first performing the integration over k^0 in the calculation of $\hat{J}(q^2)$. We record Eq. (3.14) of [Ce 95a]:

$$\hat{J}(q^2) = -n_c n_f \int \frac{d^3k}{(2\pi)^3}\left[\frac{m}{E(\vec{k})}\right]^2 \left\{\frac{a_1^{+-}\Gamma_1^{+-} + a_2^{+-}\Gamma_2^{+-}}{q^0 - 2E(\vec{k}) + i\epsilon} - \frac{a_1^{-+}\Gamma_1^{-+} + a_2^{-+}\Gamma_2^{-+}}{q^0 + 2E(\vec{k})}\right\} \ , \quad (6.3.5)$$

where $E(\vec{k}) = (\vec{k}^2 + m^2)^{1/2}$, and where the Γ^{+-} and Γ^{-+} parametrize the confinement vertex calculated there. In Eq. (6.3.5), $a_2^{+-} = a_2^{-+} = 4E^2 9\vec{k})/3m^2$. The corresponding integral, without confinement, is obtained from Eq. (6.3.5) by putting $\Gamma^{+-} = \Gamma^{-+} = m/\vec{k}^2$ and $\Gamma_2^{+-} = \Gamma_2^{-+} = 1$ [Ce 95a]. (Note that the arguments of the various Γ's are q^0 and $|\vec{k}|$ in the frame where $\vec{q} = 0$.) For $|\vec{k}| > 0.7$ GeV, we have $\Gamma^{+-} = \Gamma^{-+} = m/\vec{k}^2$ and $\Gamma_2^{+-} = \Gamma_2^{-+} = 1$. Thus, the integral over $|\vec{k}|$ in Eq. (6.3.5) only receives contributions if $|\vec{k}| \leq 0.7$ GeV. (That is, we may extend the integral over large values of $|\vec{k}|$, once $|\vec{k}| > 0.7$ GeV, without changing the result.)

Note that $\hat{J}(q^2)$ is real and that we may drop the $i\epsilon$ in the denominator of the first term of Eq. (6.3.5). That follows, since $\Gamma_1^{+-}(q, |\vec{k}|)$ and $\Gamma_2^{+-}(q, |\vec{k}|)$ are equal to zero at the on-mass-shell point, where $q^0 = 2E(\vec{k})$. We see that the cut that would have been present for $q^2 > 4m^2$ has been eliminated, when using our model of confinement.

6.4. Discussion

It is useful to compare the results obtained in Section 6.3 for $\bar{J}(q^2)$ with a subtracted function. Let us define

$$\hat{J}_{sub}(q^2) = \hat{J}_{(\rho)}(q^2) - \hat{J}_{(\rho)}(0) \quad . \tag{6.4.1}$$

The function $\hat{J}_{(\rho)}(q^2)$ was shown in Fig. 6.2 and was taken from [Ga 96b]. (Note that, in the calculation of $\hat{J}_{(\rho)}(q^2)$, we used the regularization scheme that involved the cutoffs Λ_E and Λ_3. Thus, this function makes no reference to the Pauli-Villars regularization procedure that was used when defining $\tilde{J}_{(\rho)}(q^2) \equiv J_m(q^2) - J_M(q^2)$, or $\bar{J}_{(\rho)}(q^2) \equiv \hat{J}_m(q^2) - J_M(q^2) = \tilde{J}(q^2) + [\hat{J}_m(q^2) - J_m(q^2)]$.

The function $\hat{J}_{sub}(q^2)$ is shown in Fig. 6.4 as a solid line. We see that $\hat{J}_{sub}(0) = 0$, as follows from Eq. (6.4.1). In Fig. 6.4, we also show the function $\bar{J}(q^2)$, calculated with $M = 0.62$ GeV and $m = 0.260$ GeV. The calculated value of $\bar{J}(0)$ was equal to -0.0045 GeV^2. That quite small nonzero value has its origin in the various approximations used in calculation of the confining vertex, $\Gamma^\mu(q, k)$. In Fig. 6.4, we have made $\bar{J}(q^2)$ consistent with the gauge invariance constraint, $\bar{J}(0) = 0$, by adding 0.0045 GeV^2 to the calculated values. The fact that the two curves of Fig. 6.4 are quite similar lends some justification for the subtraction procedure that was used when a regularization scheme that did not respect gauge invariance was introduced [Vo 92, Kl 92, Ce 95a].

To understand the role of confinement in the calculation of the vacuum polarization diagrams, we compare $\hat{J}_{sub}(q^2)$ and $\mathrm{Re}\tilde{J}(q^2)$ in Fig. 6.5. There, we see the rapid rise in the value of $\mathrm{Re}\tilde{J}(q^2)$ near the threshold value of $q^2 = 4m^2 = 0.27$ GeV^2.

Since $\hat{J}_{sub}(q^2)$ contains the effects of confinement, the unitarity $q\bar{q}$ cut is absent. Therefore, there is no rapid rise seen for $q^2 \simeq 4m^2$ in the case of $\hat{J}_{sub}(q^2)$. (As noted earlier, $\bar{J}(q^2)$ will have an imaginary part for $q^2 > 4M^2 = 1.54$ GeV^2, since we did not include confinement in the calculation of those diagrams where m was replaced by the regulator mass, M.)

In summary, we have shown that a subtraction procedure used previously appears to be in accord with a more fundamental approach to the maintenance of gauge invariance in the regularization of the integrals of the NJL model. [See Fig. 6.4.] We have seen rather clearly, how our model of confinement removes the unphysical quark-antiquark unitarity cut. We have also see how the q^2-dependence of the integrals considered here undergoes significant modification in the presence of confinement. [See Fig. 6.5, where we compare Re$\bar{J}(q^2)$ and $\hat{J}_{sub}(q^2)$.]

Tables

Table 5.1. Values of $g_{\rho qq}(q^2)$ and $g_{\omega qq}(q^2)$ are presented. Here $g^2_{\rho qq}(q^2) = (\tilde{m}^2_\rho - q^2)/(G_\rho^{-1} - r_1)$ and $g^2_{\omega qq}(q^2) = (\tilde{m}^2_\omega - q^2)/(G_\omega^{-1} - v_1)$, with $G_\rho = 7.12$ GeV^{-2}, $G_\omega = 7.86$ GeV^{-2}, $\tilde{m}^2_\rho = \tilde{m}^2_\omega = 1.476$ GeV^2, $r_1 = 0.0304$ GeV^2, and $v_1 = 0.0284$ GeV^2 [Ga 96b]. Note that $g_{\rho qq}(m^2_\omega) = 2.80$, $g_{\omega qq}(m^2_\omega) = 2.95$, and $g_{\rho qq}(m^2_\rho) = 2.83$..

q^2(GeV^2)	$g_{\rho qq}(q^2)$	$g_{\omega qq}(q^2)$
0.0	3.66	3.86
0.1	3.54	3.73
0.2	3.41	3.59
0.3	3.27	3.45
0.4	3.13	3.30
0.5	2.98	3.14
0.6	2.82	2.98
0.7	2.66	2.80

Figure Captions

Fig. 1.1 (a) The diagram on the left is the basic quark loop integral of the NJL model.

The propagators are $S_F(p) = (\not{p} - m_q + i\epsilon)^{-1}$, where m_q is the constituent quark mass. The additional diagrams show the introduction of a confining potential, V^C.

(b) A vertex function for the confining interaction (cross-hatched area) is given by the equation shown.

(c) Here the various terms summed in the equation of (b) are shown.

Fig. 1.2 (a) The basic quark-loop integral of the NJL model is shown. In the notation of this work we have $P^2 = t$. [See Eq. (1.1.3).]

(b) The function $\hat{J}_S(P^2)$ is defined by introducing a vertex (cross-hatched area) for the confining interaction V^C. See [Ce 95b] for a detailed discussion of the construction of such vertex functions.

(c) The function $K_S(P^2)$ is defined by the diagram shown. (See [Ce 93b].)

(d) The function $\hat{K}_S(P^2)$ is defined by including a vertex function for the confining interaction (cross-hatched region). (See [Ce 95b].)

Fig. 2.1. The dashed line and the solid line for $t < 0$ denote the values of $J_S(t)$ calculated in a Euclidean momentum space with $\Lambda_E = 1.0$ GeV. The solid line for $t > 0$ represents the result of a calculation of $\hat{J}_S(t)$ in Minkowski space. There, a three-dimensional cutoff of $\Lambda_3 = 0.702$ GeV is used for all the momentum vectors in the integral. We use $\kappa = 0.2$ GeV^2, $m_q = 262$ MeV, $G_S = 7.91$ GeV^{-2}. Note that the inclusion of the confinement vertex function would hardly affect the result for $t < 0$.

Fig. 2.2. The values of $\hat{J}_{(\omega)}(t)$ are shown for three values of κ.

a) $\kappa = 0.16$ GeV^2,

b) $\kappa = 0.22$ GeV^2,

c) $\kappa = 0.28$ GeV^2.

The dotted line represents the value of $m_\omega^2 = (0.783 \text{ GeV})^2$. The intersections of the dotted line with the solid lines yields $1/G_\omega$ for the various values of κ.

Fig. 2.3. The values of $\hat{J}_{(\rho)}(t) + \text{Re}\,\hat{K}_{(\rho)}(t)$ are shown for various κ.

a) $\kappa = 0.16$ GeV^2,

b) $\kappa = 0.22$ GeV^2,

c) $\kappa = 0.28$ GeV^2.

The dotted line denotes the value of $m_\rho^2 = (0.770\ \text{GeV})^2$. The intersection of the dotted line with the solid line yields the value of $1/G_\rho$. Note that $\hat{J}_{(\rho)}(t) = \hat{J}_{(\omega)}(t)$. (From our study of omega exchange we have fixed $\kappa = 0.22\ \text{GeV}^2$.)

Fig. 2.4. Values of Re $\hat{K}_{(\rho)}(t)$ are shown for several values of κ.

a) $\kappa = 0.16\ \text{GeV}^2$,

b) $\kappa = 0.22\ \text{GeV}^2$,

c) $\kappa = 0.28\ \text{GeV}^2$.

Fig. 3.1. (a) The nucleon-nucleon interaction in the boson-exchange model is set equal to an interaction that is defined in terms of the quark-quark T matrix.

(b) Leading diagrams in $1/n_c$ are considered as discussed in [Sh 95b].

(c) The T matrix t_{qq}, expressed in terms of the integrals $\hat{J}(t)$ and $\hat{K}(t)$ for the various channels, is used instead of the more general quark-quark T matrix of Fig. 3.1a to obtain the nucleon-nucleon interaction.

Fig. 3.2 Values of $h_\pi^{NJL}(t)$ are given by the solid line and $h_\pi^{OBE}(t)$ is represented by the dotted line. Here λ_π = 0.80 GeV and Λ_π^{OBE} = 1.3 GeV. [See Eqs. (3.1.3), (3.1.6) and (3.1.8).]

Fig. 4.1. (a) Here the wavy line represents a photon of momentum q. The lines with arrows denote quarks, while the cross-hatched area represents a nucleon "core" that is "dressed" by various mesons (ρ, ω, . . .).

(b) Here the solid dot denotes a coupling constant of the extended NJL model (G_ρ or G_ω).

(c) Here we represent the development of the bubble string of the extended NJL model. The bubble string may be replaced by a meson propagator through the use of the relation $G_\rho / \{ 1 - G_\rho [\hat{J}_{(\rho)}(q^2) + \hat{K}_{(\rho)}(q^2)] \} = - g^2_{\rho qq}(q^2) / [q^2 - m^2_\rho]$ in the case of the rho meson, for example.

(d) Via bosonization, one may introduce the omega propagator, which is represented by a double line in the figure. At the photon-meson vertex, one has a factor $m^2_\omega / g^\omega(q^2)$, where $g^\omega(q^2)$ is the momentum-dependent meson decay constant of the omega meson.

Fig. 4.2. Values of $F_1^S(q^2)$ are shown. The phenomenological values are given by the solid line, while the result of our fit using the VMD model is represented by the dashed line. Here $\lambda_1^S = 0.745$ GeV. [See Eq. (4.1.12).]

Fig. 4.3. Values of $F_2^S(q^2)$ are shown. The phenomenological values are

given by the solid line, while the dashed line shows the result of the VMD model with $\lambda_2^V = 0.70$ GeV. [See Eq. (4.1.11).]

Fig. 4.4. (a) Diagrams that are considered when using the extended NJL model to calculate the meson-exchange between two nucleon core states. The solid dot represents either G_ρ or G_ω. The "bubble string" may be summed by using the relation $G_\omega/[1 - G_\omega \hat{J}_{(\omega)}(q^2)] = -g^2_{\omega qq}(q^2)/(q^2 - m^2_\omega)$ in the case of the isoscalar $q\bar{q}$ channel, for example.

(b) The omega propagator is shown as a double line. The small filled dots denote factors of $g_{\omega qq}(q^2)$.

Fig. 4.5. The figure shows values of $f^{OBE}_{(\omega)}(q^2)$ [dashed line] and $f^{NJL}_{(\omega)}(q^2)$ [solid line]. (See Eqs. (4.3.2) and (4.3.4).)

Fig. 4.6. The figure shows values of $f^{OBE}_{(\rho)}(q^2)$ [dashed line] and $f^{NJL}_{(\rho)}(q^2)$ [sold line]. (See Eqs. (4.3.6) and (4.3.11).)

Fig. 5.1. a) The basic quark-loop integral for the NJL model is used to define the tensor $J^{\mu\nu}_{(\rho)}(q) = -\hat{g}^{\mu\nu} J_{(\rho)}(q^2)$. More precisely, the evaluation of the diagram using Feynman rules yields $-iJ^{\mu\nu}_{(\rho)}(q)$.

b) A summation of a ladder of confinement interactions (a linear potential) serves to define a confining vertex, shown as a shaded area. The diagram on the left serves to define $\hat{J}^{\mu\nu}_{(\rho)}(q) = -\hat{g}^{\mu\nu}\hat{J}_{(\rho)}(q^2)$.

c) The equation whose solution yields the confining vertex. (Solutions of this equation are described in detail in [Ce 95a].) Note that $\hat{J}_{(\rho)}(q^2) = \hat{J}_{(\omega)}(q^2)$, if $m_d = m_u$.

Fig. 5.2. Values of $\hat{J}_{(\rho)}(q^2)$ are shown for spacelike and timelike values of q^2. The calculation in the timelike region is done in Minkowski space with a cutoff on all three-momenta of $\Lambda_3 = 0.702$ GeV. The spacelike values are calculated in Euclidean momentum space with a cutoff $\Lambda_E = 1.0$ GeV. Confinement is included in the calculation made for $q^2 > 0$ and we find $\hat{J}_{(\rho)}(0) = 0.0860$ GeV^2. The Euclidean-space calculation made for $q^2 < 0$ yields $J_{(\rho)}(0) = 0.0944$ GeV^2. The dotted curve is used to interpolate between the two calculations. Note that $\hat{J}_{(\rho)}(q^2) = \hat{J}_{(\omega)}(q^2)$, if $m_d = m_u$. The quark mass in these calculations is $m_q = 262$ MeV.

Fig. 5.3. a) The diagram shown is used to define the tensor

$\hat{K}^{\mu\nu}_{(\rho)}(q) = -\hat{g}^{\mu\nu}(q)K_{(\rho)}(q^2)$. Here the wavy lines represent pions. (In analogy to the comment made in the caption to Fig. 5.1, we note that the evaluation of such diagrams using Feynman rules yields $-iK^{\mu\nu}_{(\rho)}(q)$.)

b) Introduction of the confining vertex of Fig. 1c serves to define the tensor $\hat{K}^{\mu\nu}_{(\rho)}(q) = -\hat{g}^{\mu\nu}\hat{K}_{(\rho)}(q^2)$. Note that $\hat{K}_{(\rho)}(q^2) \gg \hat{K}_{(\omega)}(q^2)$, since the two-pion decay of the omega violates G-parity.

Fig. 5.4. Values of $\hat{J}_{(\omega)}(q^2)$ are presented for several values of q^2 and for a range of values of the constituent quark mass.

a) $q^2 = 0.0\ \text{GeV}^2$

b) $q^2 = 0.10\ \text{GeV}^2$

c) $q^2 = 0.20\ \text{GeV}^2$

d) $q^2 = 0.60\ \text{GeV}^2$

Here $\kappa = 0.22\ \text{GeV}^2$ and $\Lambda_3 = 0.702\ \text{GeV}$. Note that $\hat{J}_{(\omega)}(q^2) = \hat{J}_{(\rho)}(q^2)$, if $m_d = m_u$. Further, $\hat{J}_{(\omega)}(q^2)$ decreases when the constituent mass is increased. Therefore, $\left[\hat{J}_{(\omega)}(q^2, m_u) - \hat{J}_{(\omega)}(q^2, m_d)\right] > 0$, since $m_d > m_u$.

Fig. 5.5. a) The diagrammatic element that serves to define $\hat{J}^{\mu\nu}_{(\rho\omega)}(q) = -\hat{g}^{\mu\nu}\hat{J}_{(\rho\omega)}(q^2)$ is shown. The shaded triangular area represents the confining vertex of Fig. 5.1c. The small open circles denote the coupling constants, G_ρ or G_ω, of the NJL

model. (See Eq. (5.1.1.)

b) The calculation of the mixed correlation function $\hat{\Pi}^{\mu\nu}_{(\rho\omega)}(q) = -\hat{g}^{\mu\nu}(q)\hat{\Pi}_{(\rho\omega)}(q^2)$ is shown. Each diagram contains a single factor of $\hat{J}_{(\rho\omega)}(q^2)$ and a varying number of factors of $\hat{J}_{(\rho)}(q^2)$ and $\hat{J}_{(\omega)}(q^2)$, with the $\hat{J}_{(\rho)}(q^2)$ factors to the left of $\hat{J}_{(\rho\omega)}(q^2)$ and the $\hat{J}_{(\omega)}(q^2)$ factors to the right of $\hat{J}_{(\rho\omega)}(q^2)$ in the diagram.

Fig. 5.6. Values of $\hat{J}_{(\rho\omega)}(q^2)$ are shown. Here $m_d = 262$ MeV, $m_u = 260$ MeV, $\kappa = 0.22$ GeV^2 and $\Lambda_3 = 0.702$ GeV. Note that κ is the string tension and Λ_3 is the cutoff on the magnitude of all three-momenta in a Minkowski-space calculation of the quark-loop integrals. At the origin, we have $\hat{J}_{(\rho\omega)}(0) = 0.628 \times 10^{-4}$ GeV^2. Note that $J_{(\rho)}(q^2) = 0$ for $q^2 = -0.45$ GeV^2. Values for spacelike q^2 were obtained using the formalism presented in the Appendix. (Values for $m_d^0 - m_u^0 = 2.69$ MeV are obtained by multiplying the values in the figure by 2.69/2.)

Fig. 5.7 Values of $\bar{\theta}_3(q^2)/\bar{\theta}_3(m_\omega^2)$ are shown as a dashed line. [See Eq. (5.5.3). Here, the meson widths appearing in Eq. (5.5.3) were neglected.] We recall that $\theta_3(m_\omega^2) = \bar{\theta}_3(m_\omega^2)$. Here $m_d^0 - m_u^0 = 2.0$ MeV. (See the caption of Fig. 5.6.)

Fig.6.1 a) The fundamental loop-integral of the NJL model that serves to define the tensor $-iJ^{\mu\nu}(q)$. Here the quark propagators are $S(k) = [\not{k} + m + \epsilon]^{-1}$, where m is the constituent quark mass.

b) The vertex function, $\Gamma^{\mu}(q, k)$, that sums a ladder of confining interactions is shown as a filled triangular area. The driving term is γ^{μ} in the case of the omega meson and $\gamma^{\mu}\tau_3$ in the case of the rho.

c) The loop integral that defines the tensor $-i\hat{J}^{\mu\nu}(q)$ is shown. Note that $\hat{J}^{\mu\nu}(q)$ is real, since the vertex function vanishes if both quarks go on mass shall simultaneously.

Fig. 6.2 Values of $\hat{J}(q^2) = \hat{J}_{(\rho)}(q^2)$ are shown. (This figure may be found in Ref. [Ga 96b].) For $q^2 < 0$, confinement was neglected and the calculation was done in a Euclidean momentum space, with $\Lambda_E = 1.0$ GeV. For $q^2 > 0$, confinement was taken into account. The calculation was made in Minkowski space with a cutoff on all three-momenta in the loop integral of $\Lambda_3 = 0.702$ GeV [Ga 96b]. The dotted curve serves to interpolate between the two calculations.

Fig.6.3 a) The figure serves to define $-\bar{J}^{\mu\nu}(q)$ as the difference between a quark loop integral (including confinement) and the loop integral with the Pauli-Villars regulator mass, [See Eq. (6.3.1).]

(Propagators with the mass M are shown as lines with a large filled circle imposed. We have not included confinement for such propagators.)

b) The figure depicts Eq. (6.3.2) in a schematic fashion. The value of the first bracket in Fig. 6.3b may be obtained using the procedures described in [Sh 97b]. (See Section 6.2 for analytic expressions for the first bracket.) Note that the calculation of the second bracket does not require regularization. (See Section 6.3.)

Fig. 6.4 The dotted curve represents $\bar{J}(q^2)$ of Eq. (6.3.2), while the continuous line represents the value of $\hat{J}_{sub}(q^2) = \hat{J}_{(\rho)}(q^2) - \hat{J}_{(\rho)}(0)$. The calculation of $\bar{J}(q^2)$ was made for $m = 0.260$ GeV and $M = 0.62$ GeV. [Note that $\bar{J}(q^2)$ has an imaginary part for $q^2 > 4M^2$, since we did not include the confinement vertex in the integrals containing the regulator mass M.] Values of $\hat{J}_{(\rho)}(q^2)$ were taken from [Ga 96b], where the cutoffs, Λ_E and Λ_3, were used in the regularization procedure. This figure shows the effects of confinement in the calculation of the vacuum polarization diagrams. (Note that $\mathrm{Im}\bar{J}(q^2)$ is nonzero for $q^2 > 4m^2$.)

Fig. 6.5 The dashed curve shows the value of $\bar{J}(q^2) = J_m(q^2) - J_M(q^2)$. [See Eqs. (6.2.6)-(6.2.11).] Only $\mathrm{Re}\bar{J}(q^2)$ is shown. The continuous curve represents $\hat{J}_{sub}(q^2) = \hat{J}_{(\rho)}(q^2) - \hat{J}_{(\rho)}(0)$ and is the same as the

corresponding curve shown in the calculation of $\tilde{J}(q^2)$ and $\bar{J}(q^2)$ was made with $m_q = 0.26$ GeV and $M = 0.62$ GeV.

FIGURES

Fig. 11

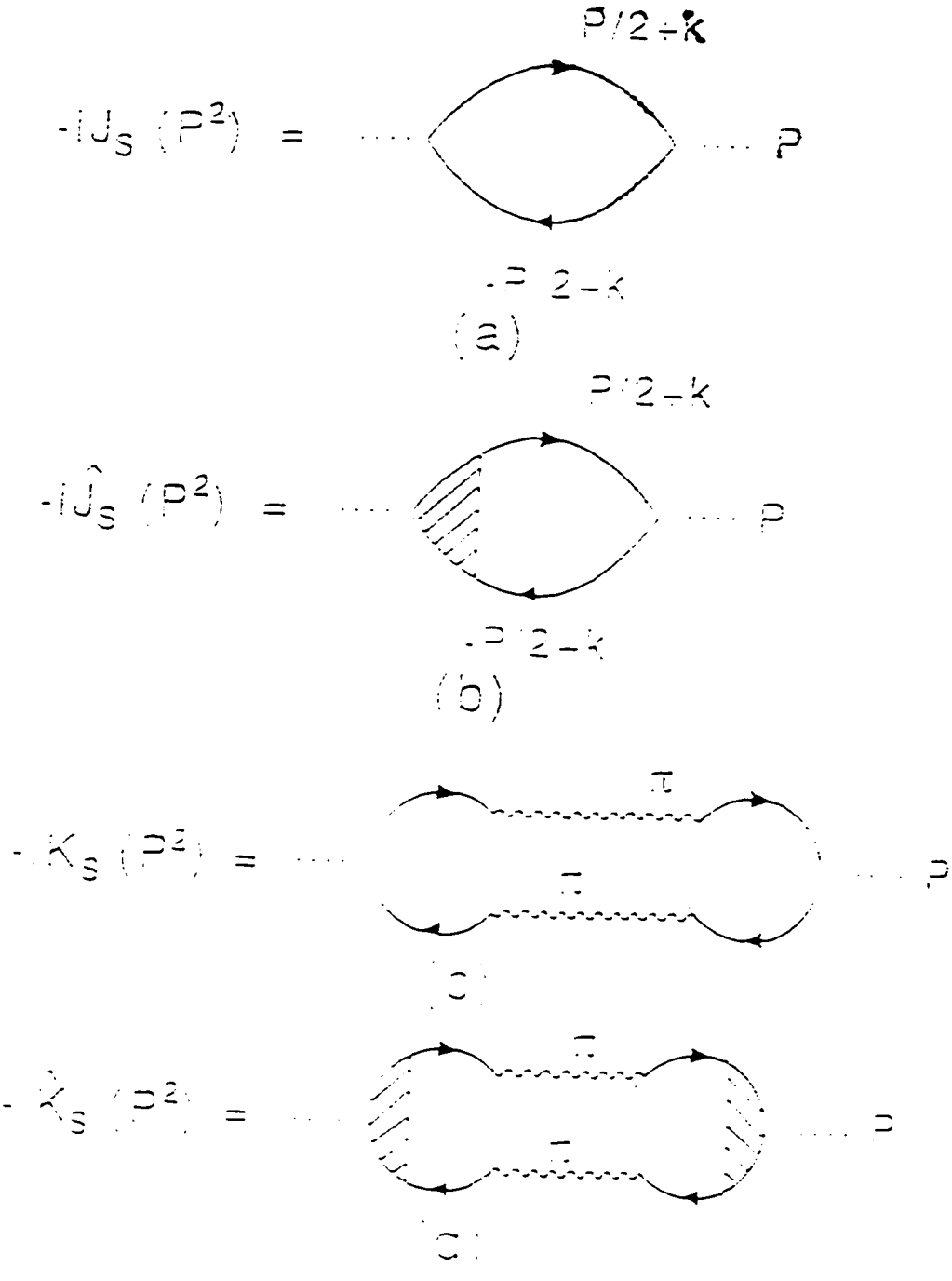

Fig 1.2

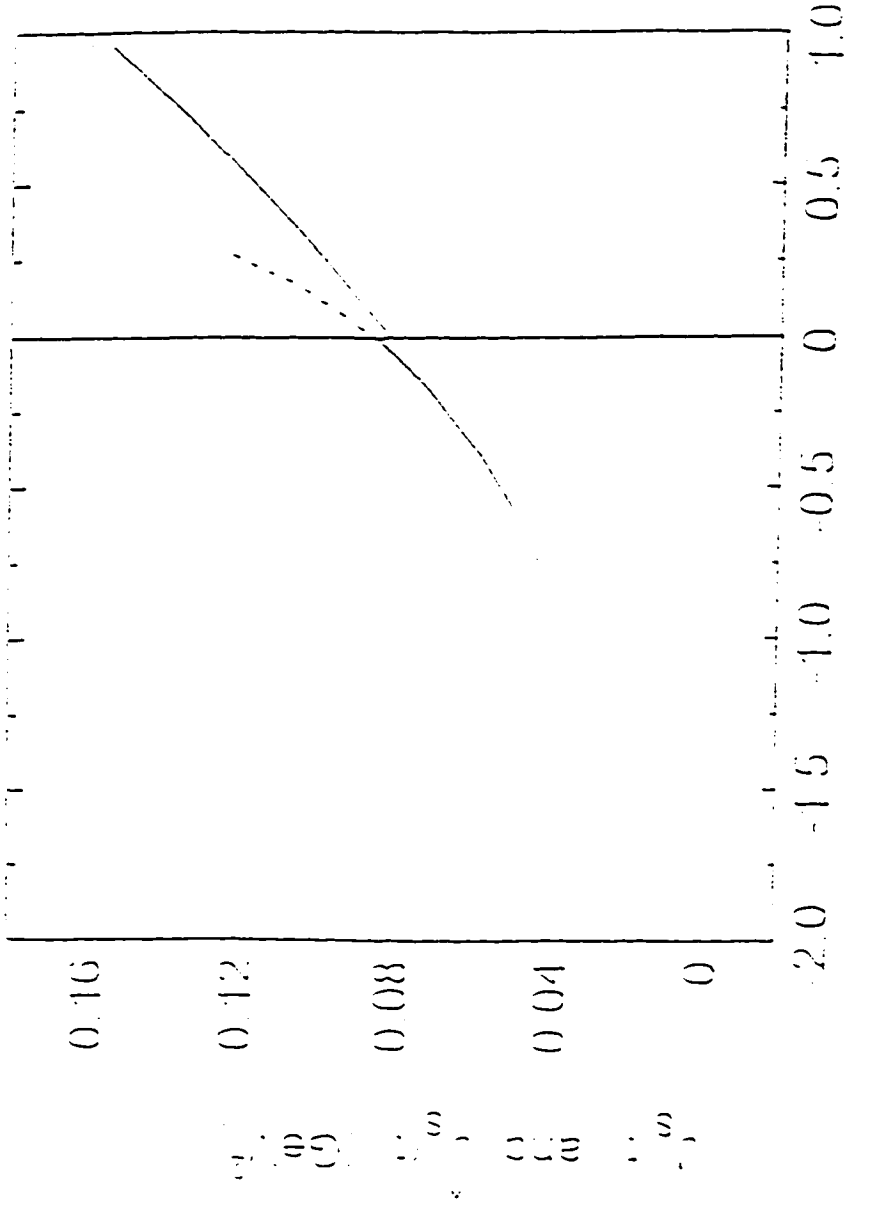

Fig. 2.1

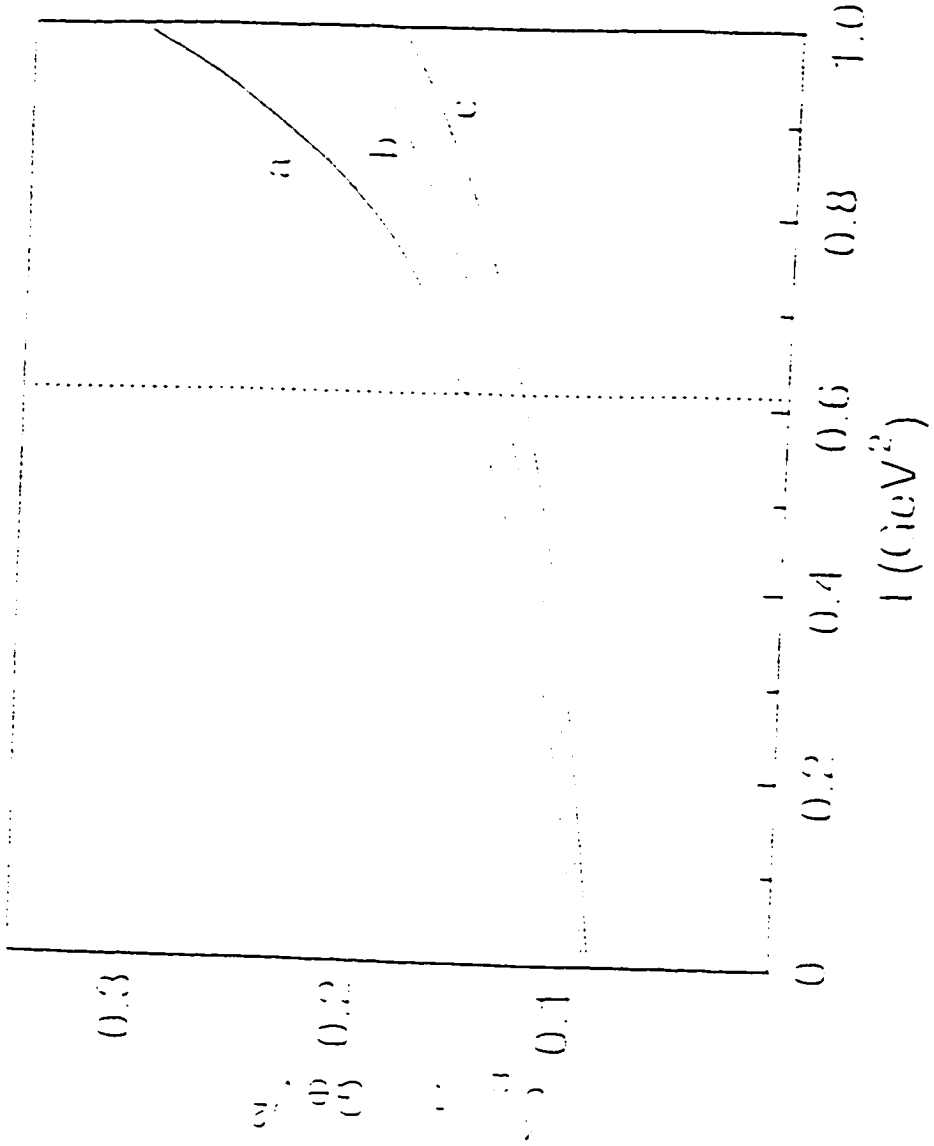

Fig. 2.2

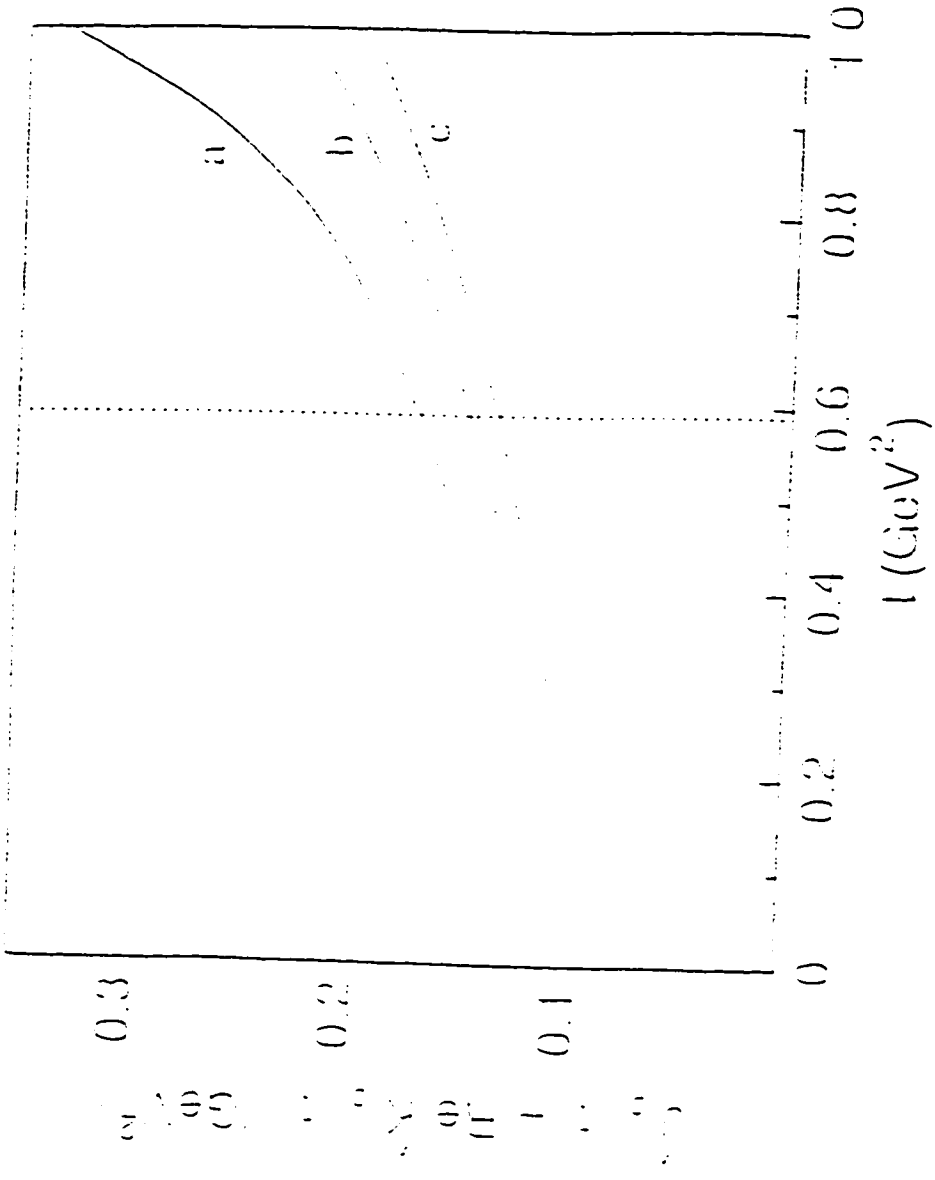

Fig 2.3

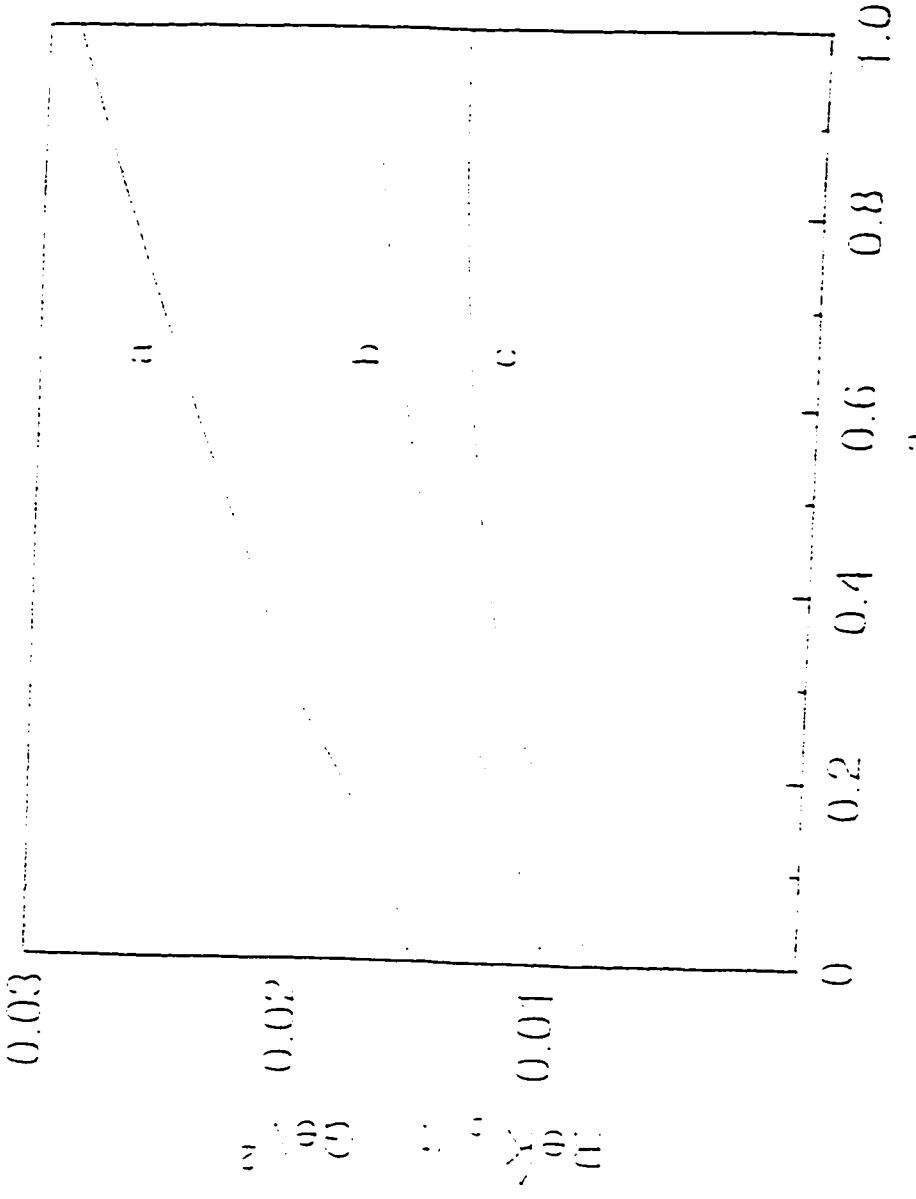

Fig. 2.4

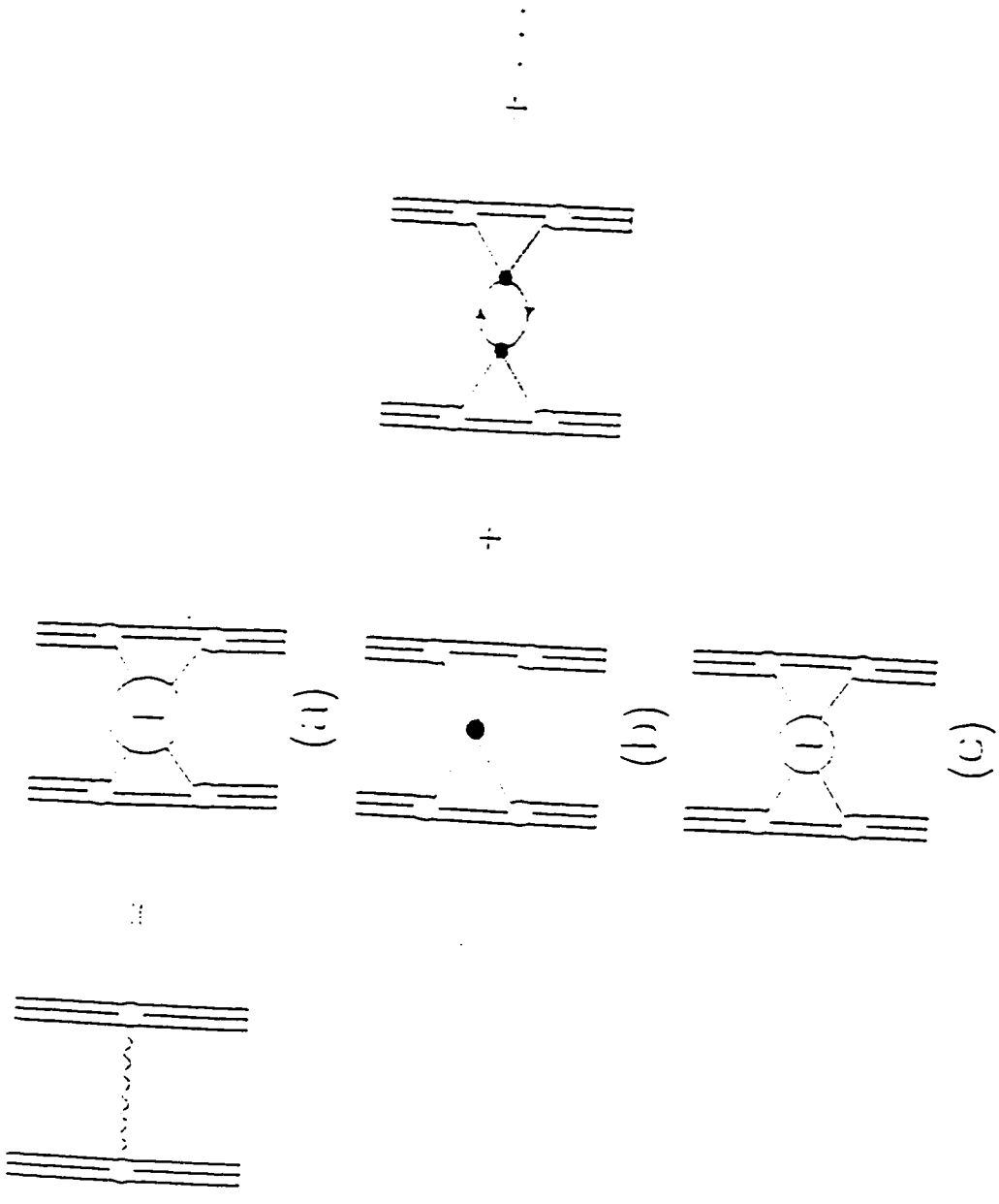

Fig. 31

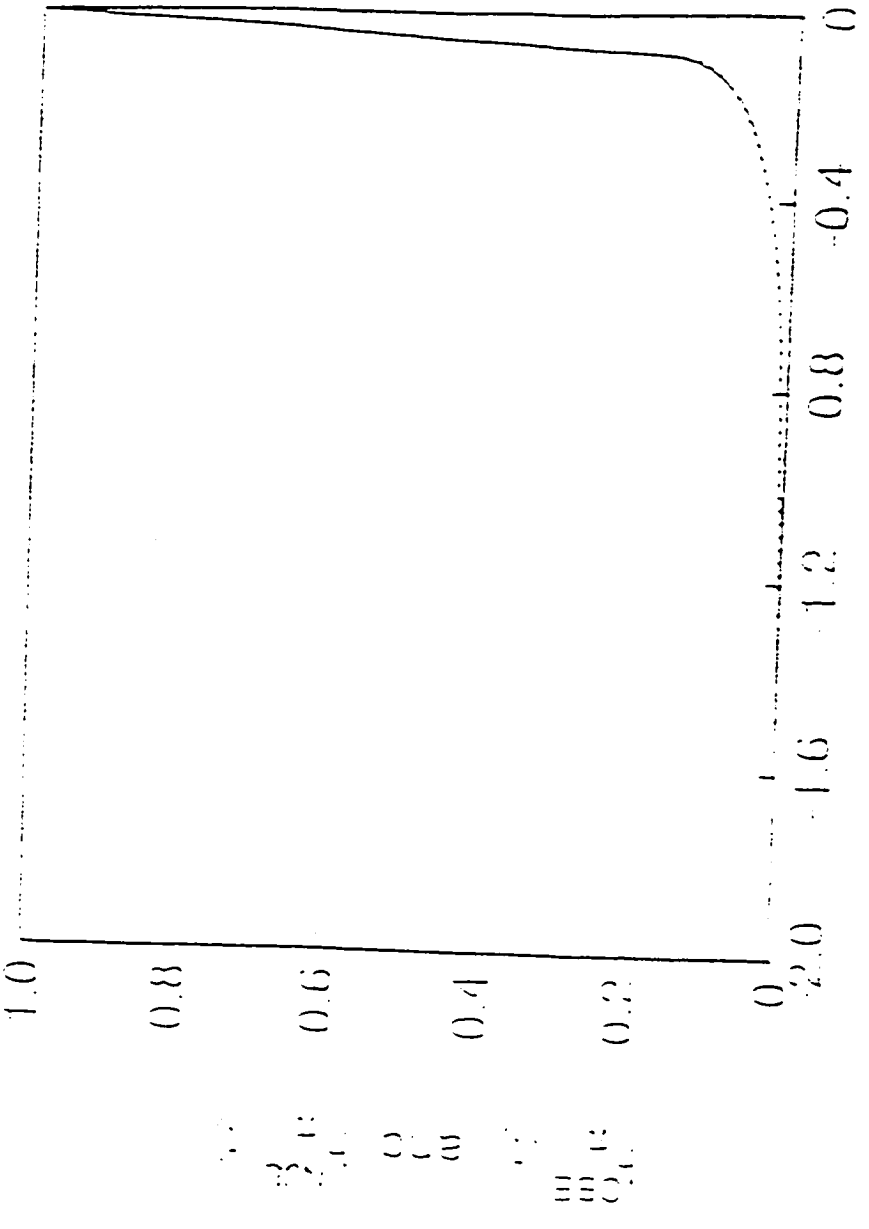

Fig. 3.2

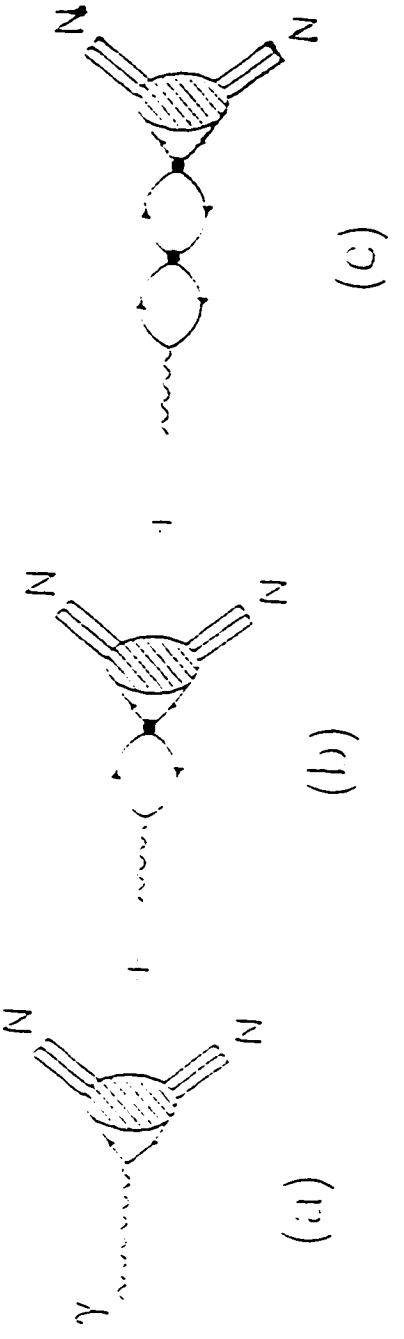

Fig. 4.1

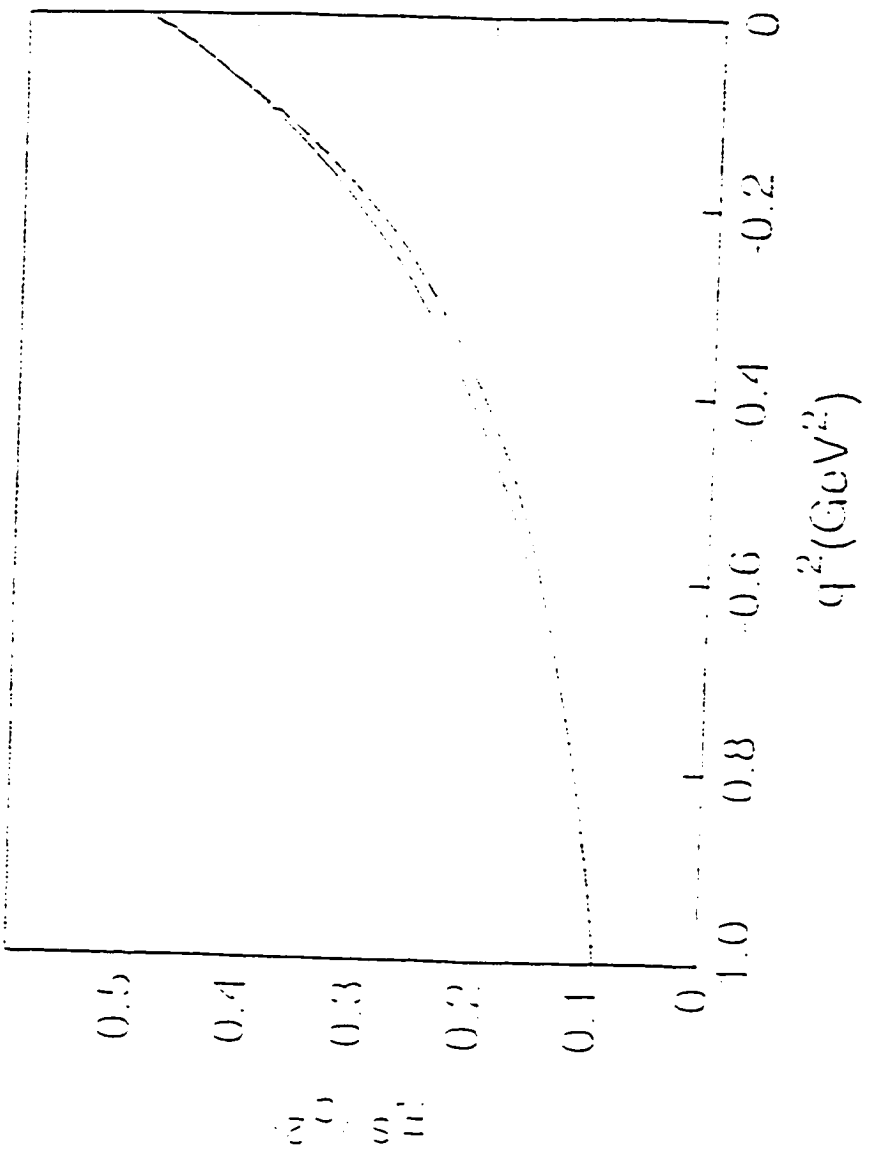

Fig 4.2

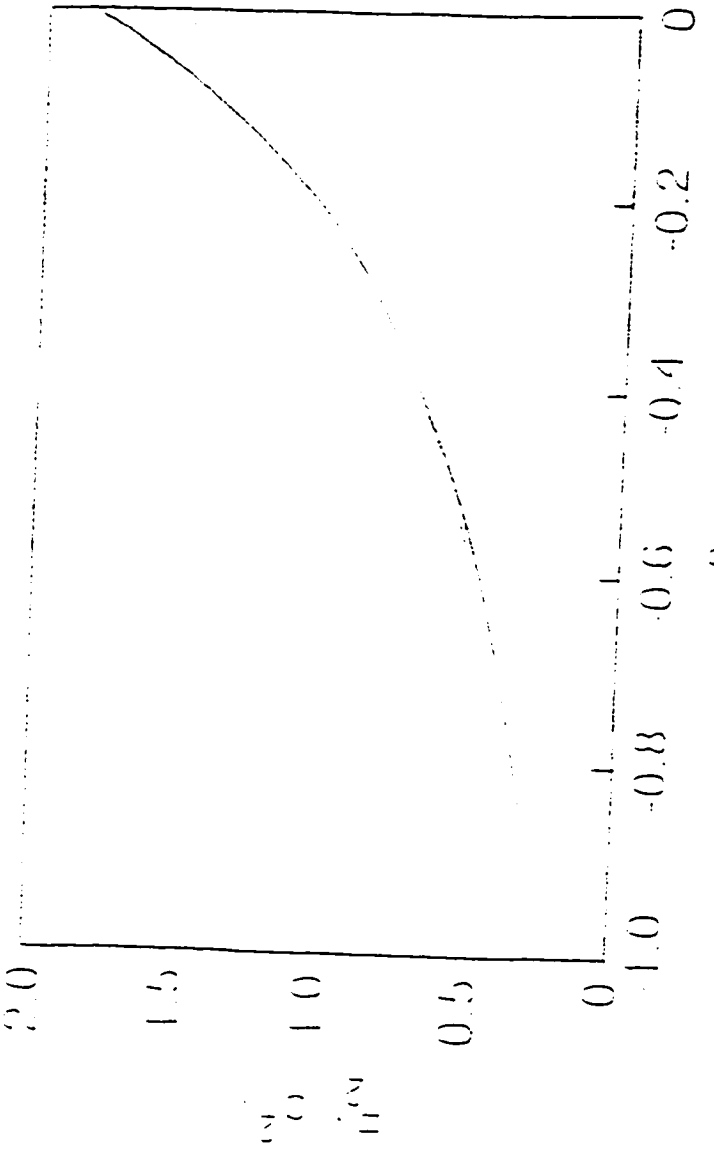

Fig. 4.3

(a) (b)

Fig. 4.4

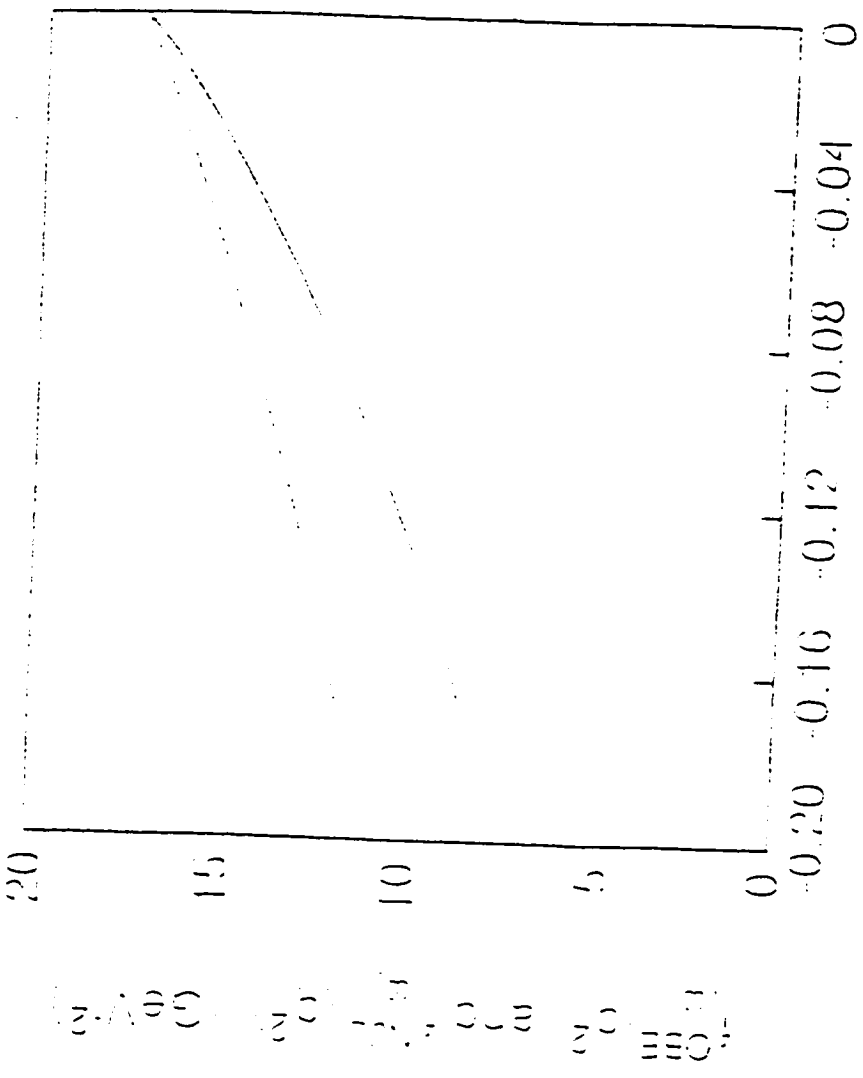

Fig 4.5

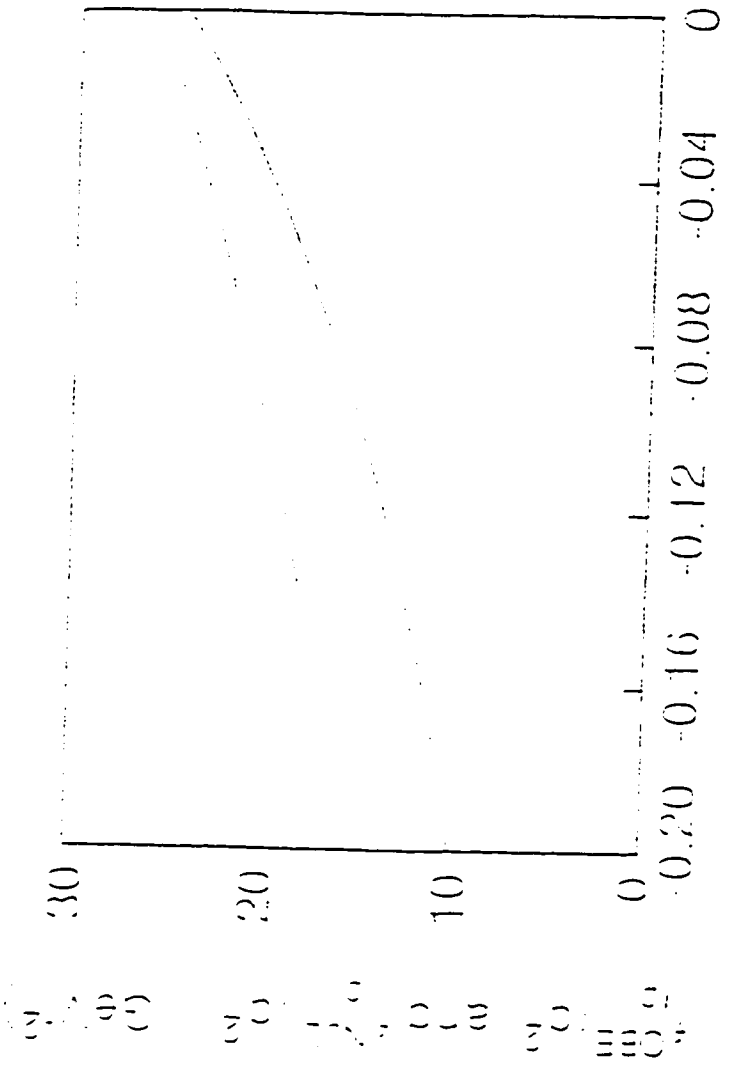

Fig 4.6

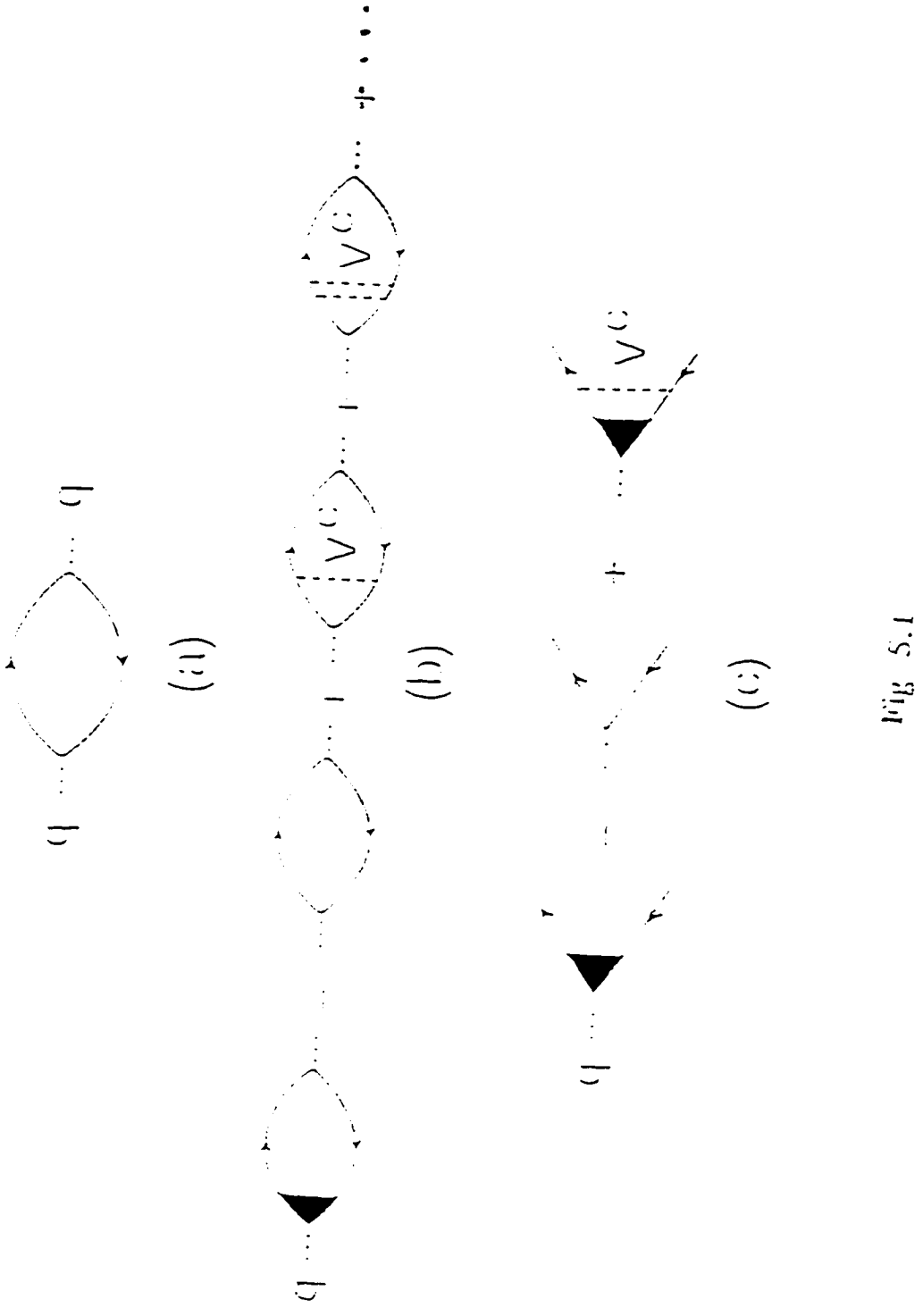

Fig 5.1

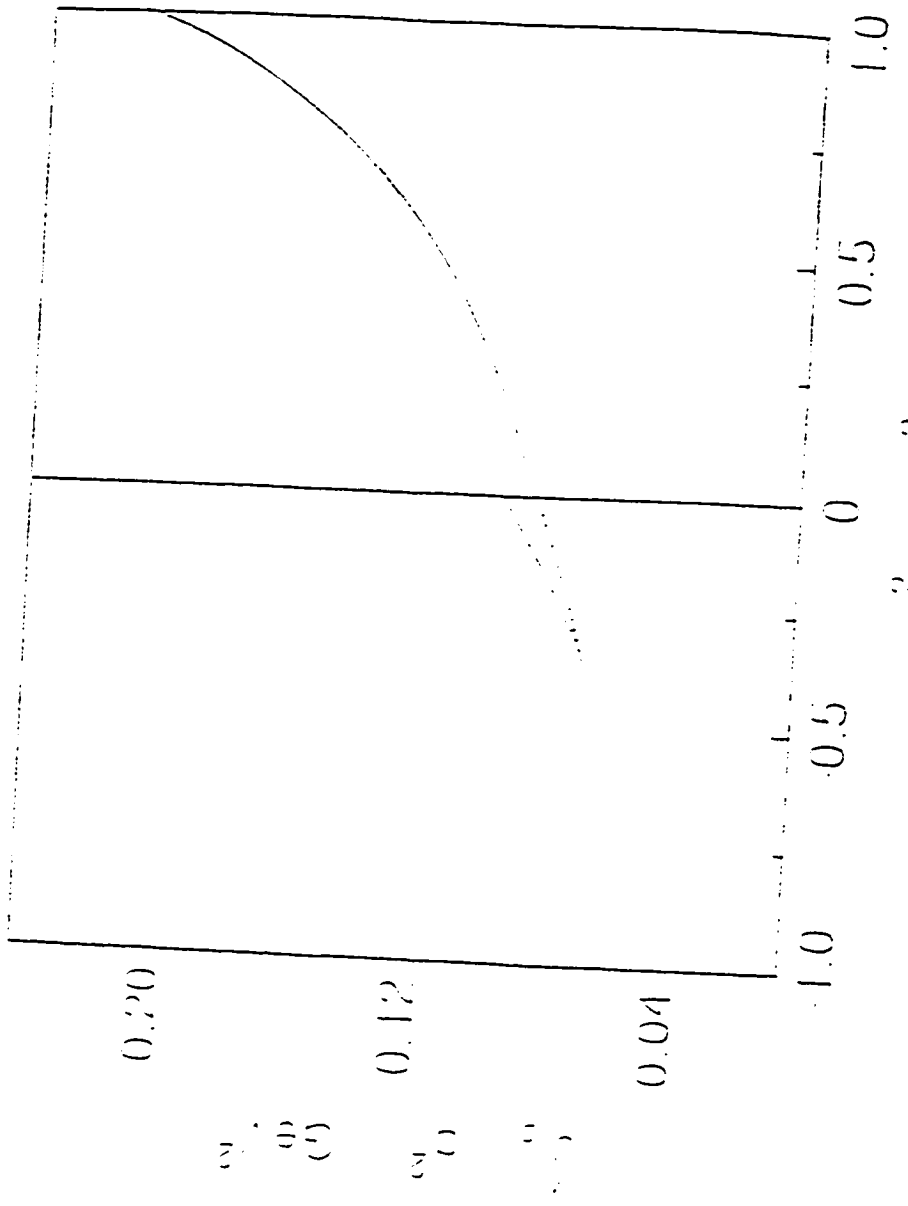

Fig. 5.2

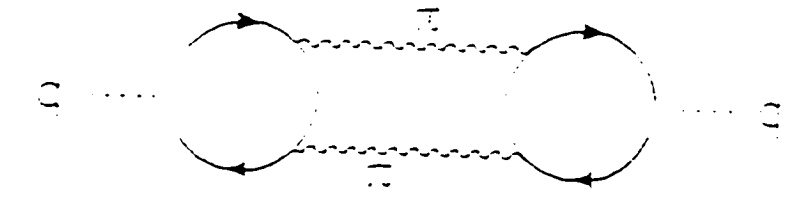

(a)

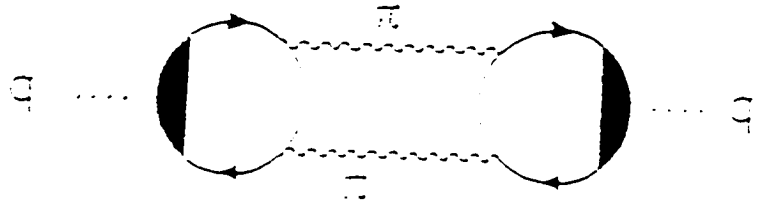

(b)

Fig 5.3

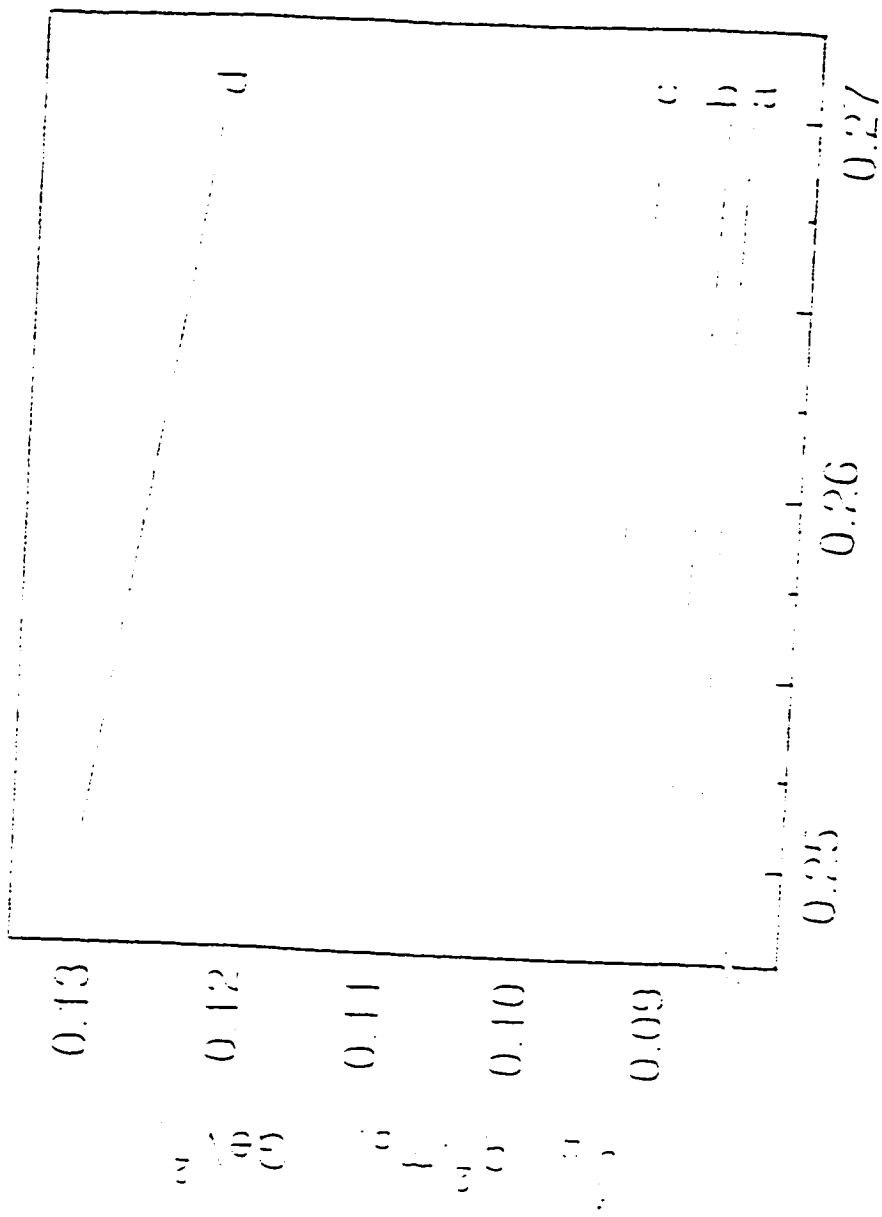

Fig. 5.4

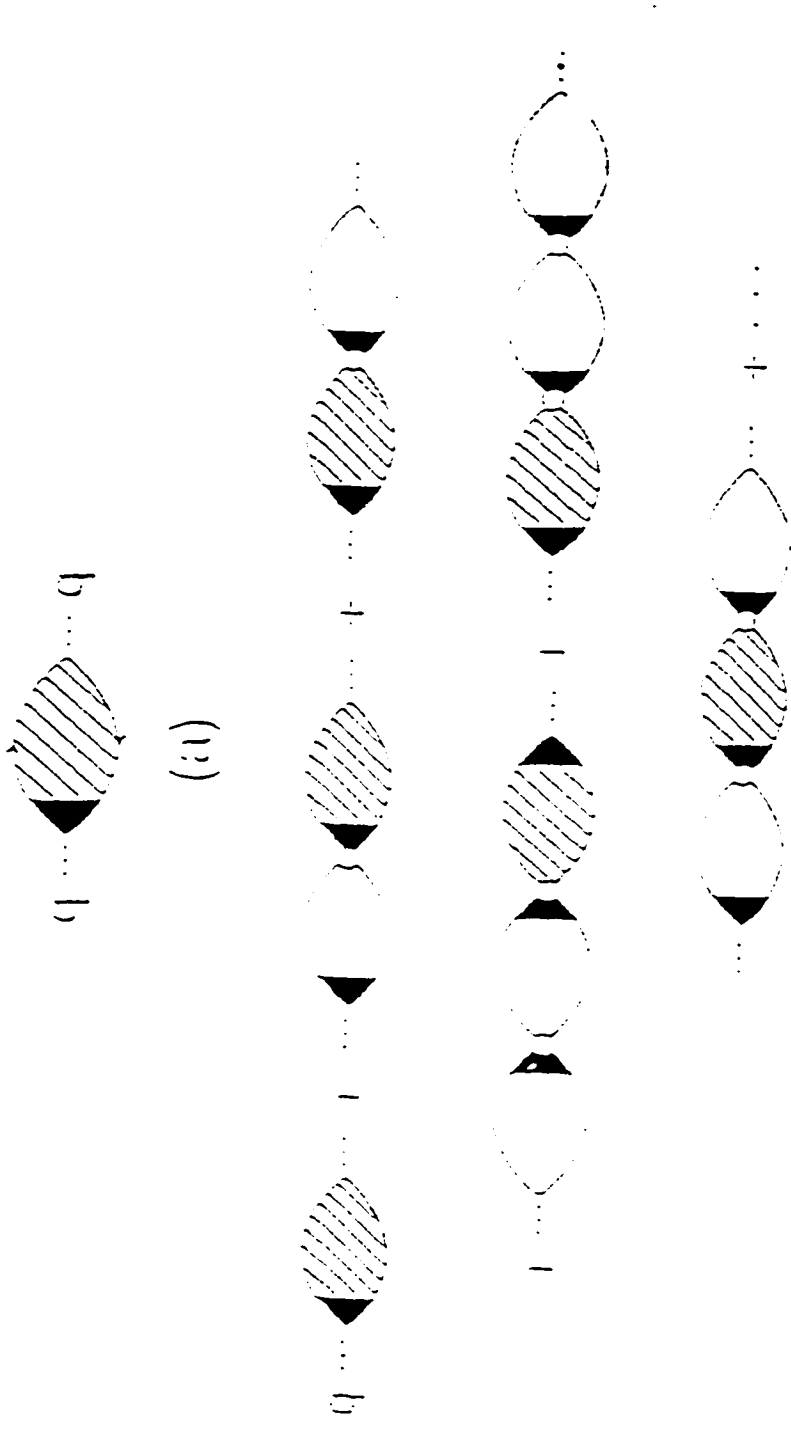

Fig 5.5

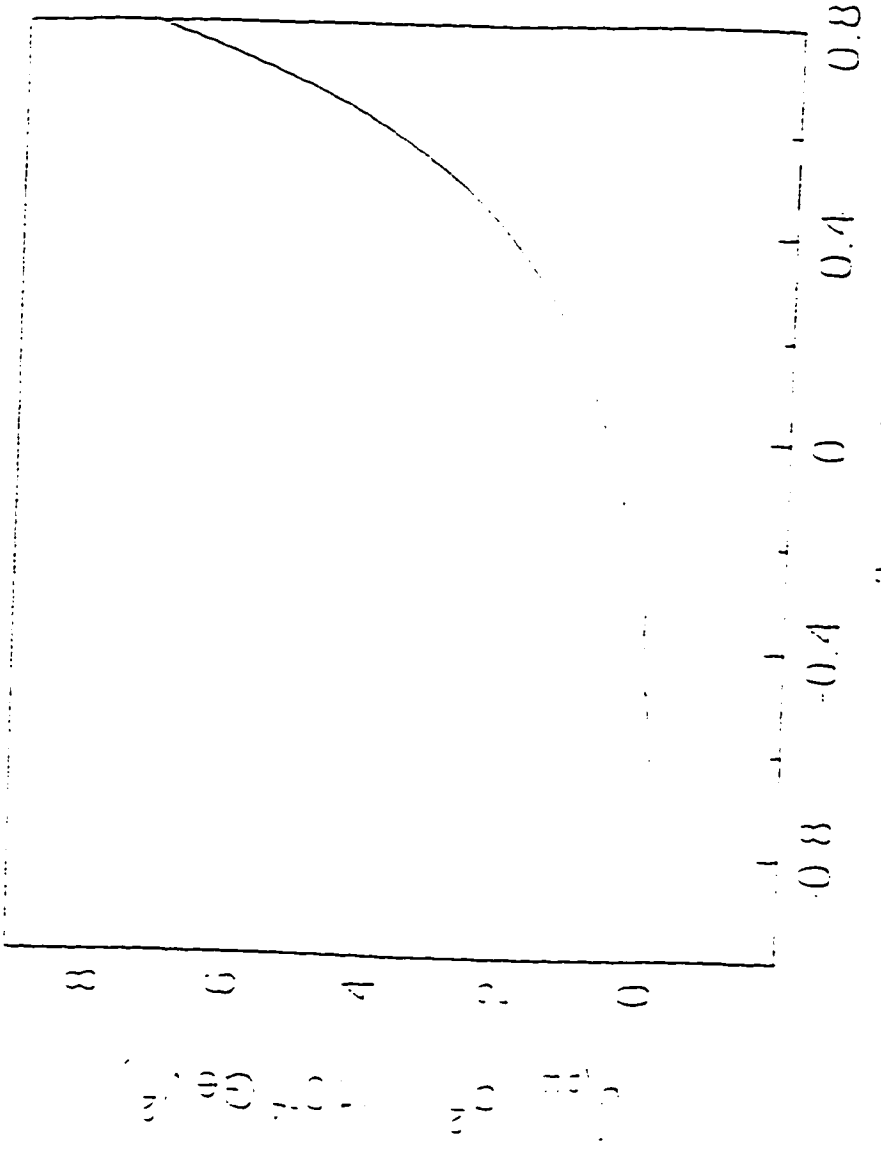

Fig. 5.6

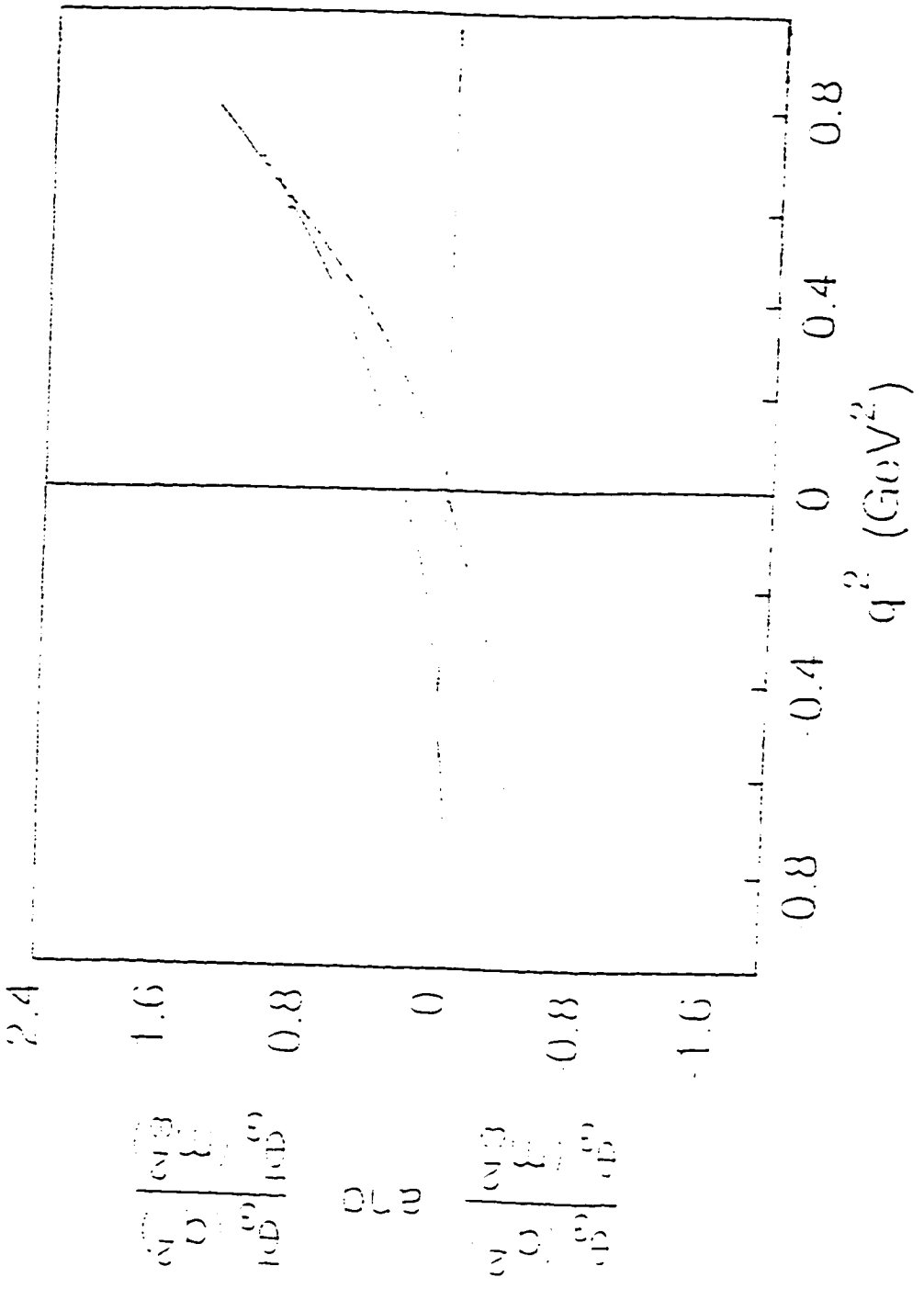

Fig. 5.7

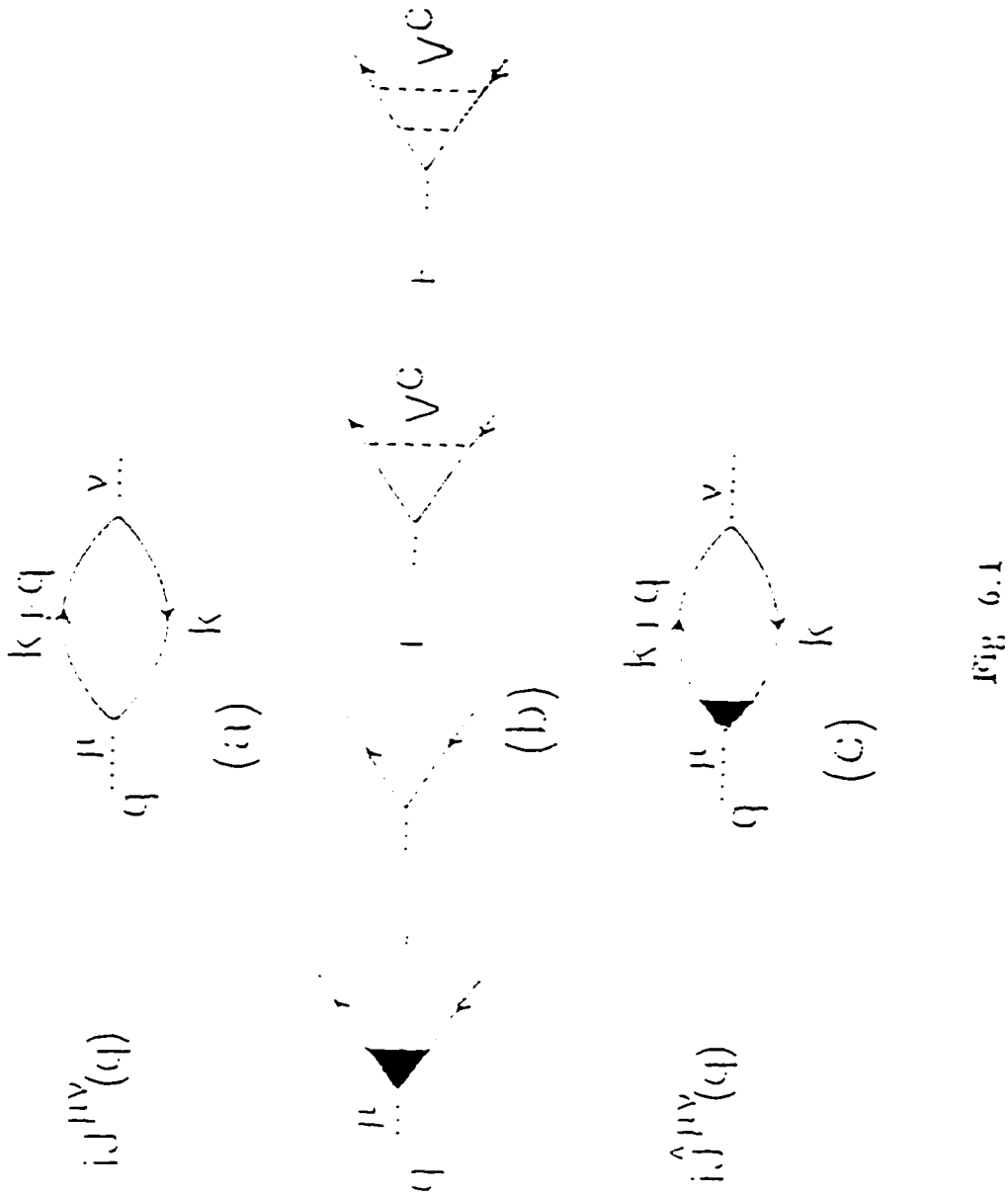

Fig. 6.1

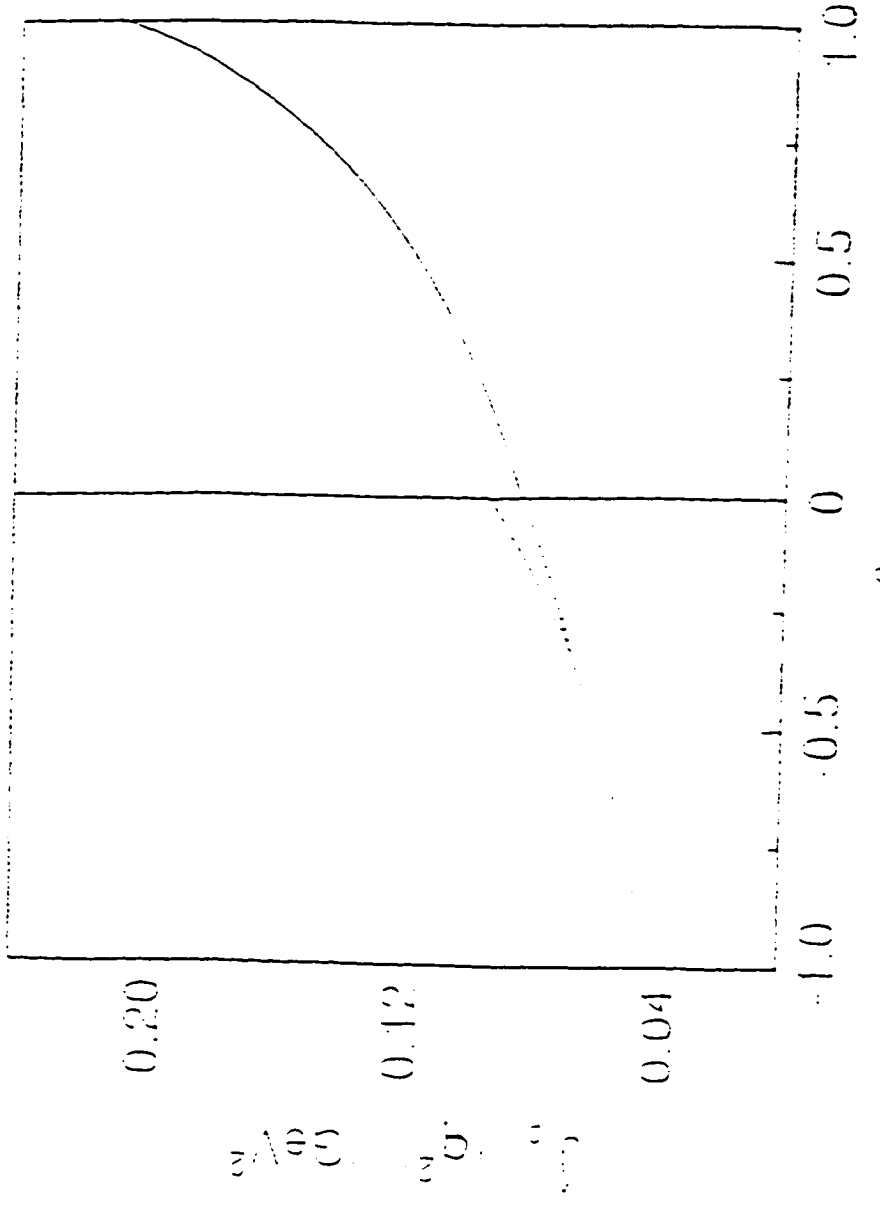

Fig 6.2

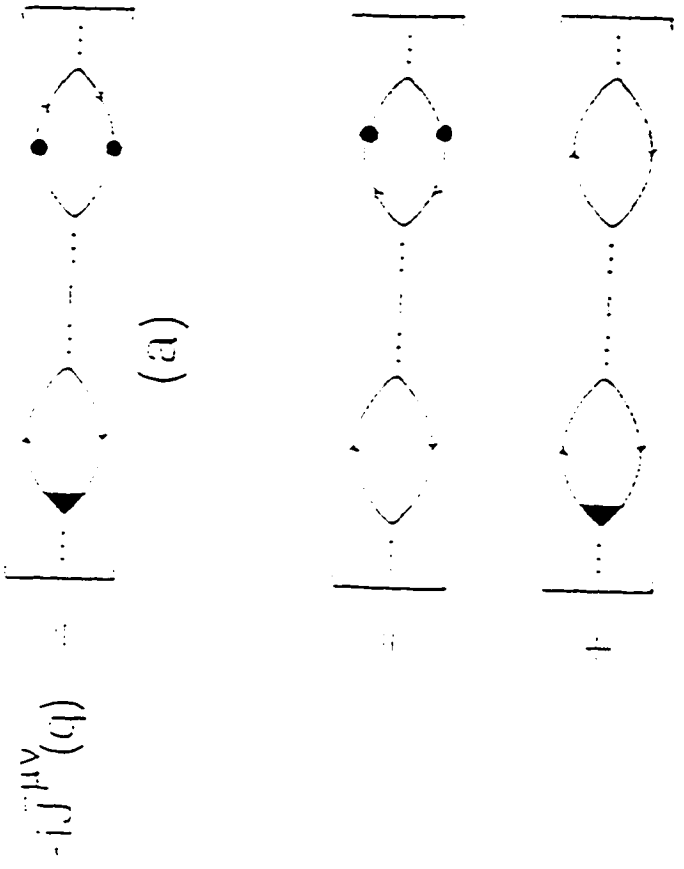

Fig 6.3

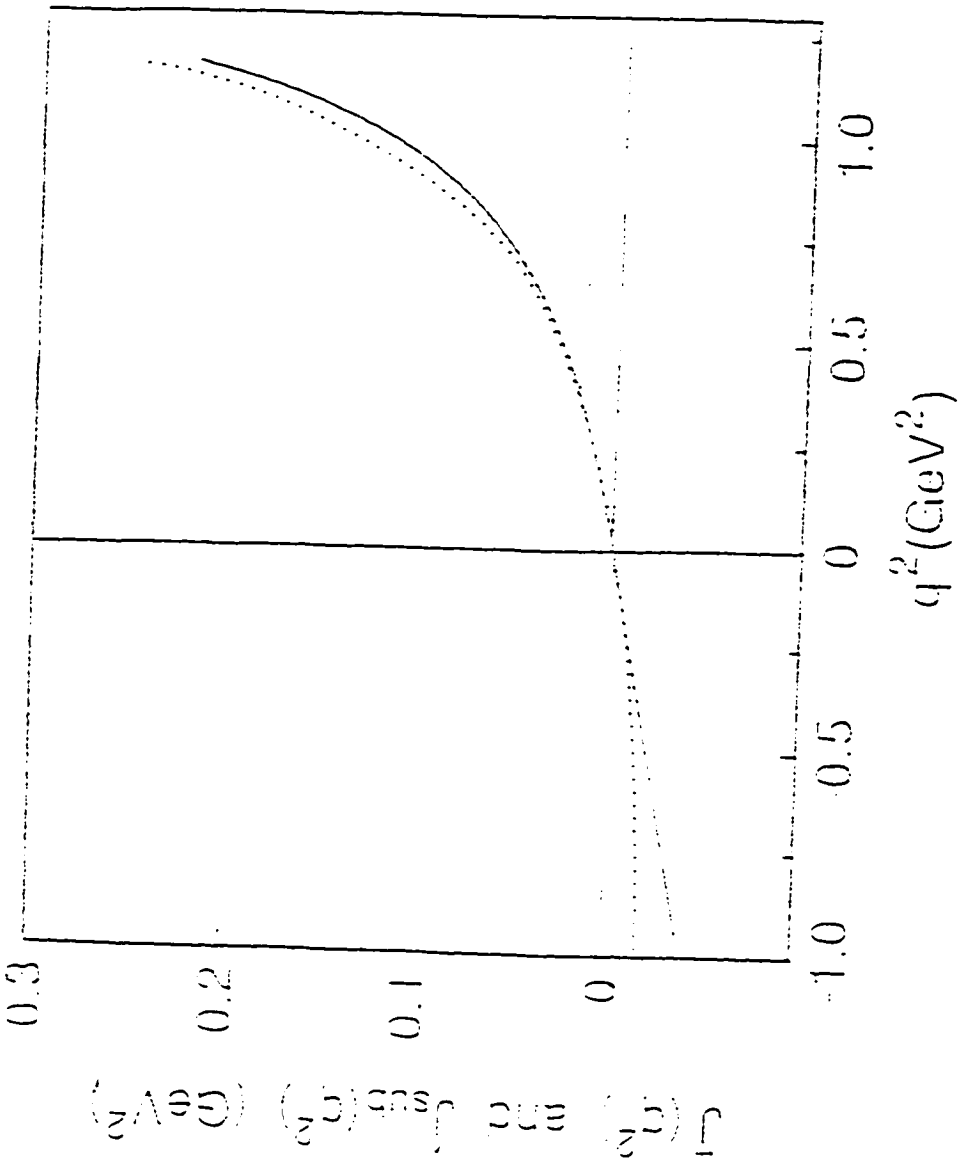

Fig 6.4

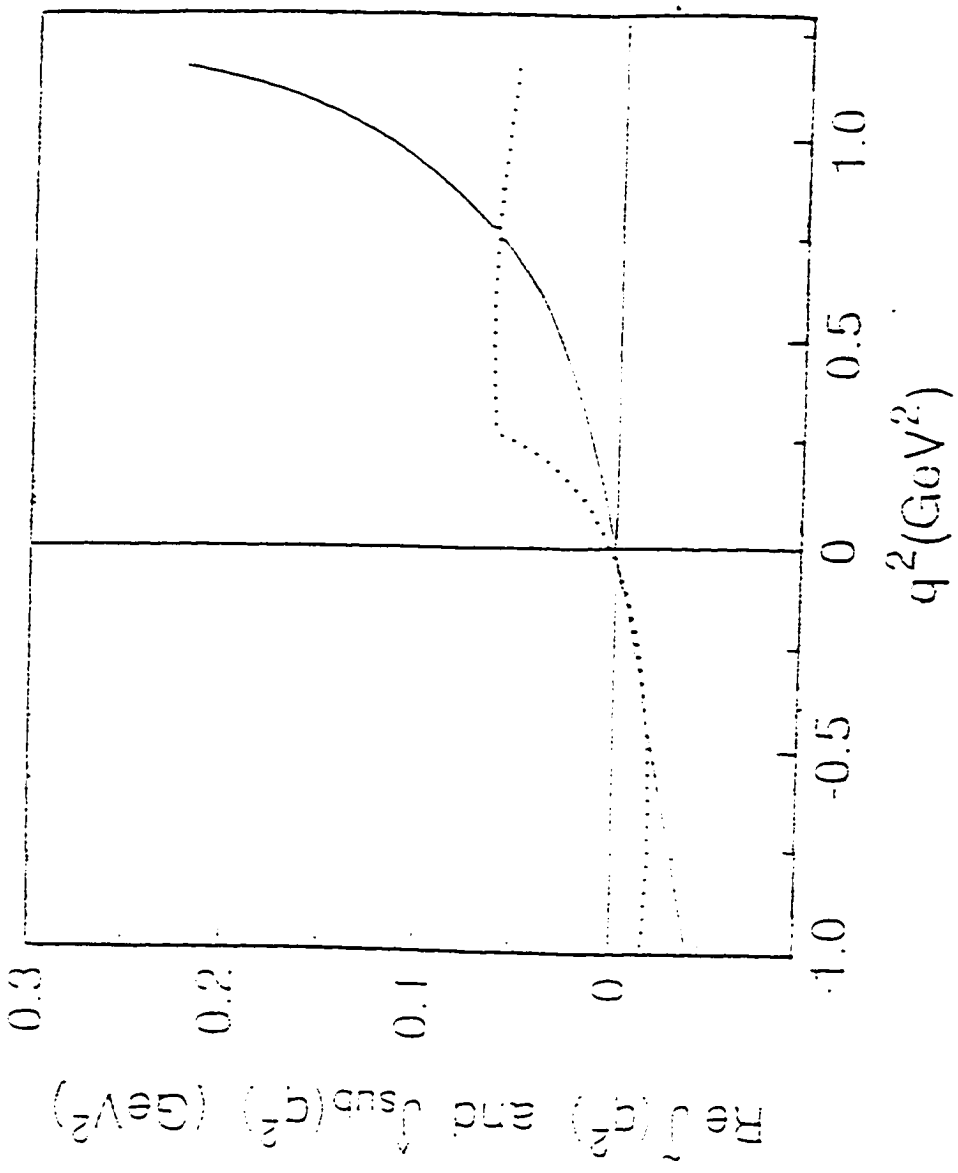

Fig 6.5

References

[Be 92] V. Bernard, A.A. Osipov and Ulf-G. Meissner, Phys. Lett. B**285**, 119 (1992).

[Ca 92] Nan-Wei Cao, C.M.Shakin and Wei-Dong Sun, Phys. Rev. C**46**, 2535 (1992).

[Ce 85] L.S. Celenza, A. Rosenthal, and C.M. Shakin, Phys. Rev. C**31**, 212 (1985).

[Ce 93a] L.S.Celenza, C.M.Shakin, Wei-Dong Sun and Xiquan Zhu, Phys. Rev. C **48**, 159(1993).

[Ce 93b] L.S.Celenza, C.M.Shakin, Wei-Dong Sun, J.Szweda, and Xiquan Zhu, International Journal of Modern Physics E **2**, 603 (1993).

[Ce 95a] L.S. Celenza, C.M. Shakin, Wei-Dong Sun, J. Szweda and Xiquan Zhu, Ann. Phys.(N.Y.) **241**,1 (1995).

[Ce 95b] L.S.Celenza, C.M.Shakin, Wei-Dong Sun, J.Szweda, and Xiquan Zhu, Phys. Rev. D**51**, 3638 (1995).

[Ce 95c] L.S.Celenza, C.M. Shakin, Wei-Dong Sun and J. Szweda, Phys. Rev. C**51**, 3372(1995).

[Co 95] T.D. Cohen and G.A. Miller, Univ. of Washington preprint (1995).

[Du 83] D. Dumbrais, et al., Nucl. Phys. B**216**, 277 (1983).

[Fr 95] R. Friedrich and H. Reinhardt, Nucl. Phys. A**594**, 406 (1995).

[Ga 96b] Shun-fu Gao, L.S. Celenza, C.M. Shakin, Wei-Dong Sun and J. Szweda,

Phys. Rev. C**53**, 1936 (1995).

[Go 92] T. Goldman, J.A. Henderson, and A.W. Thomas, Few-Body Systems **12**, 123(1992).

[Ha 94] T. Hatsuda, E.M. Henley, Th. Meissner, and G. Krein, Phys. Rev. C**49**, 452(1994).

[Iq 95] M.J. Iqbal, Xuemin Jin, and Derek B. Leinweber, TRIUMF preprint: TRI-PP-94-47(1995).

[Ka 93] Michio Kaku, Quantum field theory (Oxford University Press, New York, 1993).

[Kl 90] S. Klimt, M. Lutz, U. Vogl and W. Weise, Nucl. Phys. A**516**, 429 (1990).

[Kl 92] S.P. Klevansky, Rev. Mod. Phys. **64**, 649 (1992).

[Ma 89] R. Machleidt, in Advances in Nuclear Physics, Vol. 19, eds. J.W. Negele and E. Vogt(Plenum, New York, 1989). (See Tables A.1 and A.2.)

[Ma 95] Kim Maltman, preprint (York University, Dept. of Mathematics, North York, Ontario, Canada, 1995).

[Mi 94] K.L. Mitchell, P.C. Tandy, C.D. Roberts, and R.T. Cahill, Phys. Lett. B**335**, 282(1994).

[Mc 75] P.C. McNamee, M.D. Scadron, and S.A. Coon, Nucl. Phys. A**249**, 483 (1975).

[Na 61] Y. Nambu and G. Jona-Lasinio, Phys. Rev. **122**, 345 (1961); **124**, 246 (1961).

[Oc 94] H.B. O'Connell, B.C. Pearce, A.W. Thomas, and A.G. Williams, Phys. Lett. B**336**,1 (1994).

[Oc 95] H.B. O'Connell, B.C. Pearce, A.W. Thomas, and A.G. Williams, Phys. Lett. B**354**,14 (1995).

[Sh 95a] C.M. Shakin, Wei-Dong Sun and J. Szweda, Ann. Phys. (N.Y.) **241**, 37 (1995).

[Sh 95b] C.M. Shakin, Wei-Dong Sun and J. Szweda, Phys. Rev. C**52**, 3353 (1995).

[Sh 97a] C.M. Shakin, Wei-Dong Sun , to be published in Phys. Rev. C. (1997).

[Sh 97b] C.M. Shakin, Wei-Dong Sun , to be published in Phys. Rev. D. (1997).

[Vo 92] U. Vogl and W. Weise, Prog. Part. Nucl. Phys. **27**, 195 (1992).